

1 **To What Extent Do DNN-based Image Classification**
2 **Models Make Unreliable Inferences?**

3 **Yongqiang Tian · Shiqing Ma · Ming Wen ·**
4 **Yepang Liu · Shing-Chi Cheung · Xiangyu**
5 **Zhang**

6
7 Received: date / Accepted: date

Please note that this is a post-peer-review, pre-copyedit version of an article published in Empirical Software Engineering (accepted in 2021). The final authenticated version is available online at: <http://dx.doi.org/10.1007/s10664-021-09985-1> This is the accepted manuscript version and it is only for the authors' self-archiving.

Yongqiang Tian
Department of Computer Science and Engineering
The Hong Kong University of Science and Technology
Hong Kong, China
E-mail: ytianas@cse.ust.hk

Shiqing Ma
Department of Computer Science
Rutgers University
Piscataway, NJ, USA
E-mail: shiqing.ma@rutgers.edu

Ming Wen
School of Cyber Science and Engineering
Huazhong University of Science and Technology
Wuhan, Hubei, China
E-mail: mwenaa@hust.edu.cn

Yepang Liu
Department of Computer Science and Engineering
Southern University of Science and Technology
Shenzhen, Guangdong, China
E-mail: liuyp1@sustech.edu.cn

Shing-Chi Cheung
Department of Computer Science and Engineering
The Hong Kong University of Science and Technology
Hong Kong, China
E-mail: scc@cse.ust.hk

Xiangyu Zhang
Department of Computer Science
Purdue University
West Lafayette, IN, USA
E-mail: xyzhang@purdue.edu

Abstract Deep Neural Network (DNN) models are widely used for image classification. While they offer high performance in terms of accuracy, researchers are concerned about if these models inappropriately make inferences using features irrelevant to the target object in a given image. To address this concern, we propose a metamorphic testing approach that assesses if a given inference is made based on irrelevant features. Specifically, we propose two metamorphic relations (MRs) to detect such unreliable inferences. These relations expect (a) the classification results with different labels or the same labels but less certainty from models after corrupting the relevant features of images, and (b) the classification results with the same labels after corrupting irrelevant features. The inferences that violate the metamorphic relations are regarded as unreliable inferences.

Our evaluation demonstrated that our approach can effectively identify unreliable inferences for single-label classification models with an average precision of 64.1% and 96.4% for the two MRs, respectively. As for multi-label classification models, the corresponding precision for MR-1 and MR-2 is 78.2% and 86.5%, respectively. Further, we conducted an empirical study to understand the problem of unreliable inferences in practice. Specifically, we applied our approach to 18 pre-trained single-label image classification models and 3 multi-label classification models, and then examined their inferences on the ImageNet and COCO datasets. We found that unreliable inferences are pervasive. Specifically, for each model, more than thousands of correct classifications are actually made using irrelevant features. Next, we investigated the effect of such pervasive unreliable inferences, and found that they can cause significant degradation of a model’s overall accuracy. After including these unreliable inferences from the test set, the model’s accuracy can be significantly changed. Therefore, we recommend that developers should pay more attention to these unreliable inferences during the model evaluations. We also explored the correlation between model accuracy and the size of unreliable inferences. We found the inferences of the input with smaller objects are easier to be unreliable. Lastly, we found that the current model training methodologies can guide the models to learn object-relevant features to certain extent, but may not necessarily prevent the model from making unreliable inferences. We encourage the community to propose more effective training methodologies to address this issue.

Keywords Deep Learning · Metamorphic Testing · Software Engineering for AI

1 Introduction

Deep Neural Network (DNN) models have been widely deployed for image classification tasks (Krizhevsky et al. 2012; Simonyan and Zisserman 2015; He et al. 2016; Howard et al. 2017; Zoph et al. 2018). While these models outperform classic algorithms, such as SIFT+FV (Sanchez and Perronnin 2011) and Sparse Coding (Lin et al. 2011), in terms of classification accuracy (Krizhevsky et al. 2012), which is the proportion of the inputs in test set whose inference result is the same as the ground truth, recent studies have raised concerns about other properties of such models, including reliability (Ribeiro et al. 2016; Moosavi-Dezfooli et al. 2016; Stock and Cissé 2018), fairness (Tramèr et al. 2017; Aggarwal et al. 2019; Zhang et al. 2020a), robustness (Carlini and Wagner 2017). To help detecting the inappropriate behaviors of DNN models, various testing techniques (Xie et al. 2011;

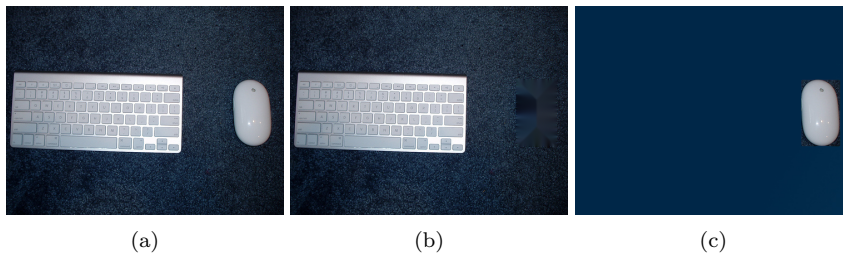


Fig. 1: (a): The Original Image. (b): Object (Mouse) Corrupting Mutation. (c): Object (Mouse) Preserving Mutation.

54 Ding et al. 2017; Pei et al. 2017; Tian et al. 2018; Zhang et al. 2018; Dwarakanath
 55 et al. 2018; Ma et al. 2018b) have been proposed. For instance, Pei et al. (Pei
 56 et al. 2017) proposed an optimization strategy to generate adversarial test inputs
 57 for image classification. Dwarakanath et al. (Dwarakanath et al. 2018) leveraged
 58 metamorphic testing to detect bugs in model implementations.

59 These techniques, however, do not consider a key property when evaluating
 60 a DNN-based image classification model, that is, whether the inferences made
 61 by the model are based on the features encoded from the target objects or the
 62 features encoded from these objects’ background. We refer to the former features
 63 as *object-relevant features*, the latter as *object-irrelevant features*, and the property
 64 as *object-relevancy property*. Intuitively, a reliable inference made by a DNN model
 65 should be mostly based on object-relevant features, instead of object-irrelevant
 66 features.

67 For instance, let us assume that the *mouse* shown in Figure 1a is the *target*
 68 *object*. The features encoded from it are object-relevant features, and the features
 69 encoded from the rest of this image are object-irrelevant. Let us further assume
 70 that a model classifies the image as shown in Figure 1a as “mouse”. This inference
 71 is reliable on the condition that it is made mostly based on the object-relevant
 72 features, instead of the object-irrelevant features. If the inference is majorly based
 73 on the object-irrelevant features but not the object-relevant features, the model
 74 is likely to classify the image in Figure 1b as “mouse” again, since this image has
 75 the same object-irrelevant features as Figure 1a. It is obvious that the image in
 76 Figure 1b does not have any “mouse” and should not be classified as “mouse”.
 77 Further, the model is also likely to classify the image as shown in Figure 1c as
 78 any label other than “mouse”, since this image does not have the object-irrelevant
 79 features in Figure 1a. It does not make sense since the image in Figure 1c clearly
 80 has the target object *mouse*.

81 Due to their stochastic nature, many DNN models do not necessarily make
 82 inferences based on object-relevant features, which may lead to various problems.
 83 For instance, a recent study showed that an animal classification model would
 84 classify any image with bright backgrounds as “wolf”, regardless of the objects in
 85 the image (Ribeiro et al. 2016). This raises the concern of reliability and overfitting
 86 for this model (Ribeiro et al. 2016; Ma et al. 2018c). Another work showed that
 87 attackers could inject a backdoor trigger, such as a yellow square in an image’s
 88 background, to a deep neural network (DNN) model (Gu et al. 2019). A model
 89 that makes inferences based on object-irrelevant features (e.g., yellow square at

the background), will then classify an image containing this trigger to a specific label, regardless of the objects in the image. Thus, such models are not robust and can cause catastrophic consequences when being deployed in mission-critical applications. Based on the above analysis, we conjecture that the violation of the object-relevancy property might be the root cause of many issues in DNN models, including but not limited to the aforementioned ones. Therefore, it is important to develop effective techniques to assess DNN models' inference results from the perspective of object relevancy, so as to help improve the trustworthiness of the models.

Validating DNN models' inference results with respect to object relevancy is challenging. It is well-known that DNN models behave as black boxes (Ribeiro et al. 2016; Pei et al. 2017). Their logic is learned from data and represented as model structures and weight values. It is non-trivial for human beings to examine the inference process of such models and check what kind of features determines the inference results. Some existing techniques (Ribeiro et al. 2016; Selvaraju et al. 2017) try to explain the inferences for individual input. However, these techniques still require manual efforts to make the final assessment for each input due to the lack of test oracles. In contrast, in our work, we first try to generate both test inputs and test oracles for DNN models, and then leverage them to identify unreliable inferences that violate the object-relevancy property automatically. However, generating test oracles is a long-standing challenge for software testing (Barr et al. 2015), especially in the testing of the deep learning systems (Pei et al. 2017; Tian et al. 2018; Pham et al. 2019; Nejadgholi and Yang 2019), where the expected probability outputted from DNN models is unknown.

To tackle these challenges, we resort to metamorphic testing (Chen et al. 1998), which has been popularly leveraged to test DNN models (Xie et al. 2011; Ding et al. 2017; Zhang et al. 2018; Dwarakanath et al. 2018). Specifically, we propose two metamorphic relations (MRs) to quantitatively assess a model's inferences from the perspective of object relevancy as follows:

- **MR-1** An image mutated by corrupting only the features of the target object(s) should lead to an inference result with different label(s), or an inference result with the same label(s) but less certainty.
- **MR-2** An image mutated by preserving the features of the target object(s) and corrupting other features should lead to an inference result with the same label(s).

The two metamorphic relations will be formally defined in Section 3. For the purpose of metamorphic testing, we designed image mutation operations to generate test inputs with respect to the two relations. Applying these operations to a given image allows us to check if the pair of the original inference and the inference on a generated mutant satisfies the metamorphic relations. Violations of such relations will be deemed as the indication of unreliable inferences. We note that applying metamorphic testing to evaluate DNN-based image classification models is not new. However, existing work (Tian et al. 2018; Zhang et al. 2018) mutates the whole image (e.g., blurring or rotating) to test the model robustness. In comparison, our MRs focus on object-relevant/irrelevant features in one input image and hence our image mutation is regional, semantic and more targeted. Besides, our goal is to assess whether an inference violates the object-relevancy property, which is a new property proposed by us.

138 To validate the effectiveness of our proposed approach, we applied it to three
139 popular DNN models trained on the ImageNet dataset and one model trained on
140 the COCO dataset (Lin et al. 2014), and then manually checked the results. The
141 evaluation results show that for single-label classification models, our approach
142 achieves an aggregated precision of 64.1% for MR-1 and 96.4% for MR-2. As for
143 multi-label classification models, the corresponding precision for MR-1 and MR-2
144 is 78.2% and 86.5%, respectively. We also investigated the reasons for the false
145 positives, and we found that they are mainly due to the inappropriate annotations
146 of the dataset.

147 We then deployed our approach with the aim of investigating the pervasiveness
148 of unreliable inferences. Specifically, we tested 18 pre-trained models for single-
149 label classification from Keras (Chollet et al. 2015b) and 3 models for multi-label
150 classification (He et al. 2016; Ben-Baruch et al. 2020). We found that for each of
151 them, more than thousands of correct classification inferences are actually unreli-
152 able, i.e., they are not made based on object-relevant features. More seriously, we
153 found that the pervasive unreliable inferences can cause significant bias on model
154 evaluation. Specifically, our experiments revealed that unreliable inferences can
155 cause significant degradation of a model’s overall accuracy, thus preventing devel-
156 opers from correctly evaluating a model and fairly comparing among models. For
157 example, after removing the unreliable inferences violating MR-2 in single-label
158 image classification, the model accuracy is 8.84% higher than the original one. We
159 also traced the ratio of unreliable inference during the model training and found
160 that the current model training methodology is ineffective in terms of reducing un-
161 reliable inferences. Besides, enhancing a model with respect to its accuracy does
162 not necessarily increase its probability to make reliable inferences. Therefore, de-
163 velopers need to design other methodologies with the aim to enhance a model’s
164 reliability, especially with respect to the object-relevancy property.

165 To summarize, this paper makes the following contributions:

- 166 1. We proposed a metamorphic testing technique to automatically assess the re-
167 liability of inferences generated by DNN models for image classification using
168 object-relevant metamorphic relations.
- 169 2. We evaluated our technique and the results show that it is effective. Our ap-
170 proach can find thousands of unreliable inferences with high precision for each
171 evaluated model.
- 172 3. We found that unreliable inferences are pervasive among a wide range of mod-
173 els. More seriously, such pervasive unreliable inferences significantly change
174 models’ performance with respect to the accuracy, thus affecting model evalu-
175 ation and comparison.
- 176 4. We explored the correlation between model accuracy and the ratio of unreliable
177 inferences, and found that the current model training strategy should be further
178 improved to help the model to learn the object-relevant features and avoid
179 making unreliable inferences.

180 2 Preliminaries

181 2.1 Metamorphic Testing

182 Metamorphic testing (Chen et al. 1998, 2018) was proposed to address the test
 183 oracle problem. It works in two steps. First, it constructs a new set of test inputs
 184 (called *follow-up inputs*) from a given set of test inputs (called *source inputs*) based
 185 on some properties that should be satisfied by the program under test. Second, it
 186 checks whether the program outputs based on the source inputs and the ones based
 187 on the follow-up inputs satisfy certain desirable properties, known as *metamorphic*
 188 *relations* (MRs).

189 For example, let us suppose p is a program implementing the $\sin()$ function.
 190 We know that the equation $\sin(\pi + x) = -\sin(x)$ holds for any numeric value
 191 x . Leveraging this knowledge, we can apply metamorphic testing to p as follows.
 192 Given a set of source inputs $I_s = \{i_1, i_2, \dots, i_n\}$, we first construct a set of follow-up
 193 inputs $I_f = \{i'_1, i'_2, \dots, i'_n\}$, where $i'_j = \pi + i_j$, $j \in [1, n]$. Then, we check whether the
 194 metamorphic relation $\forall j \in [1, n], p(i_j) = -p(i'_j)$ holds. A violation of it indicates
 195 the presence of faults in p .

196 2.2 DNN-based Image Classification

197 Image classification is a key application of DNN models. Its objective is to classify
 198 a given image into predefined labels. Popular DNN models for image classification
 199 include AlexNet (Krizhevsky et al. 2012), VGG (Simonyan and Zisserman 2015),
 200 ResNet (He et al. 2016), DenseNet (Huang et al. 2017), MobileNets (Howard et al.
 201 2017) and so on. The performance of these models is mostly evaluated based on
 202 the top-1 accuracy, which refers to the percentage of test images whose correct
 203 labels are in the top-1 (sorted according to probability) inference made by mod-
 204 els (Krizhevsky et al. 2012; Simonyan and Zisserman 2015; He et al. 2016; Huang
 205 et al. 2017; Howard et al. 2017).

206 There are two types of image classification tasks, single-label classification and
 207 multi-label classification. In single-label classification, each input is supposed to
 208 be classified into one label. Figure 2a from ImageNet (Deng et al. 2009) shows
 209 an example input that is expected to be classified into label “tiger shark”. Given
 210 an input i , the inference of a single-label classifier is a probability vector, $\mathbf{v}_i =$
 211 $[p_1, p_2, \dots, p_n]$, where n is the number of labels. Each element p_j in the \mathbf{v}_i rep-
 212 represents the probability that the input belongs to the j -th label. The sum of the
 213 elements is equal to 1, i.e., $\sum_0^n p_j = 1$. The label with the highest probability
 214 is regarded as the final classification label of this classification model given this
 215 input. MNIST (LeCun and Cortes 2010), CIFAR-10 (Krizhevsky et al. 2009), and
 216 ImageNet are common datasets for single-label classification.

217 In multi-label classification, the number of labels of each input is not limited
 218 to one. For example, Figure 2c from COCO (Lin et al. 2014) has three labels,
 219 {“person”, “motorcycle”, “airplane”}. In the classification, the inference result is
 220 regarded as correct if and only if it only contains the three labels (Tian et al.
 221 2020b; Wu and Zhu 2020). Similar to single-label classification models, given an
 222 input i , the inference of a multi-label classification model is a probability vector,
 223 $\mathbf{v}_i = [p_1, p_2, \dots, p_n]$, where n is the number of labels. Each element p_j in the \mathbf{v}_i

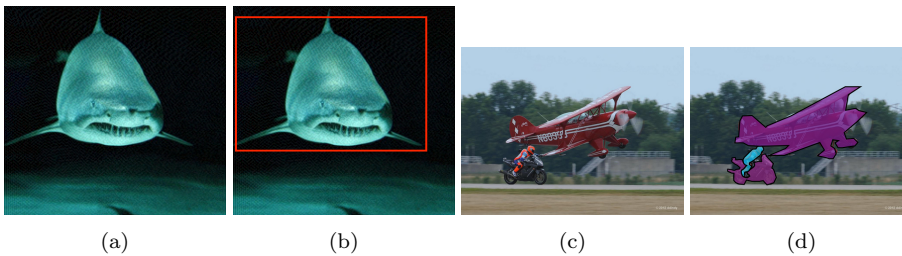


Fig. 2: Input Examples and their Annotations in Image Classifications. (a)(b): Image from the ImageNet Dataset and its Bounding Box, Label: “tiger shark”. (c)(d): Image from the COCO Dataset and its Object Mask, Labels: “person”, “motorcycle”, “airplane”.

224 represents the probability that the input belongs to the j -th label. Unlike the
 225 single-label classification model, the sum of the elements is not necessarily equal
 226 to 1, i.e., $\sum_0^n p_j \neq 1$. The final classification result is the set of labels whose
 227 probability is equal to or larger than a predefined threshold, which is usually set
 228 to 0.5 (He et al. 2016; Ben-Baruch et al. 2020). For example, given the input in
 229 Figure 2c, a multi-label classification model may output a probability vector $\mathbf{v}_i =$
 230 $[0.8, 0.7, 0.2, 0.6]$, where each element represents the probability of label “person”,
 231 “airplane”, “motorcycle” and “car”, respectively. When the threshold is set to
 232 0.5, the final classification result is {“person”, “airplane”, “car”}, which is an
 233 incorrect classification result as the “car” is not in the ground truth and the
 234 ground truth label “motorcycle” is not in the result. If the probability vector is
 235 $\mathbf{v}_i = [0.8, 0.7, 0.6, 0.2]$, the final result is {“person”, “airplane”, “motorcycle”}, and
 236 it is a correct classification result. Common multi-label datasets include COCO
 237 and Google Open Image (Krasin et al. 2017).

238 3 Object-Relevant Metamorphic Relations

239 With the aim to identify the unreliable inference made by the models based on the
 240 object-irrelevant features, we are motivated to propose two metamorphic relations
 241 as mentioned in Section 1. This section presents the details of these two relations,
 242 starting with the motivating examples. Specifically, we follow a common metamor-
 243 phic testing framework to define the two metamorphic relations (Chen et al. 1998,
 244 2018). In subsequent formulation, let $\mathcal{M}(i)$ and $\mathcal{M}(i')$ denote the inferences made
 245 by a DNN model \mathcal{M} on an input image i and its follow-up input i' , respectively.
 246 Let $\mathcal{D}(\mathcal{M}(i), \mathcal{M}(i'))$ denote the distance between two inferences $\mathcal{M}(i)$ and $\mathcal{M}(i')$.

247 3.1 MR-1

248 **Motivating Example-1** Given a source input as shown in Figure 1a, let us assume
 249 a model predicts it as “mouse”. A follow-up input is constructed by corrupting
 250 the object *mouse*, as shown in Figure 1b. After feeding the follow-up input into
 251 the previous model, one of the following two cases could happen. First, it is pos-
 252 sible that the label on follow-up input is still “mouse” and its certainty increases.

Such a situation indicates that the inference on the source input is not based on the object(*mouse*)-relevant features. If it is based on the object(*mouse*)-relevant features, it does not make sense that the model still predicts it as “mouse” when there is no such object(*mouse*). This situation is out of human expectations on image classification, as humans will not classify the follow-up image that does not have *mouse* into label “mouse” with higher certainty. Second, it is possible that the inference on the follow-up input changes to another label, or the label remains the same but the certainty decreases. In other words, due to the corruption of the object(*mouse*)-relevant features, the model cannot make the inference with the same label and the same level of certainty as the one on source input. It implies that the inference on the source input is based on the object(*mouse*)-relevant features. This situation is in line with human expectations. Since the objects have been removed or corrupted, humans are likely to classify this image to a different label, or the same label but with less certainty. Motivated by the above example, we proposed the following MR-1. In the first situation aforementioned, the MR-1 is violated while in the second situation, MR-1 is satisfied.

MR-1 An image mutated by corrupting only the features of the target object(s) should lead to an inference result with different label(s), or an inference result with the same label(s) but less certainty.

Relation Formulation of MR-1 Let i'_c be a follow-up input constructed from a source input i for a model \mathcal{M} by corrupting the target object but preserving its background. We consider such a mutation as *object-corrupting*. An example of object-corrupting mutation is shown in Figure 1a (source input) and Figure 1b (follow-up input). MR-1 mandates that $\mathcal{M}(i)$ and $\mathcal{M}(i'_c)$ should satisfy the relation: $\mathcal{D}(\mathcal{M}(i), \mathcal{M}(i'_c)) \geq \Delta_c$. Here \mathcal{D} takes two factors of $\mathcal{M}(i)$ and $\mathcal{M}(i'_c)$ into consideration, i.e., the labels in the inferences and the certainty of the inferences. The detailed definition of \mathcal{D} for MR-1 is introduced in Section 4.4.1. Δ_c denotes a threshold for the distance between two inference results made by a model under metamorphic testing using object-corrupting mutations.

Explanation of MR-1 If an inference made by a specific model is based on object-relevant features, after object-corrupting mutations, the new inference results should be affected since those object-relevant features have been corrupted, and thus those features cannot be further utilized by the model anymore. Such effects could cause two consequences. First, the model can still make the same inference as the inference of the original input while the certainty of the inference given by the model should be decreased since the object-relevant features have been corrupted. Second, the model cannot make the same inference as the inference of the original input if the corruption is very severe. Consequently, the label of the new inference should be different from the original one.

3.2 MR-2

Motivating Example-2 Given a source input shown in Figure 1a, assume a model predicts it as “mouse”. A follow-up input is constructed by preserving the object, as shown in Figure 1c. After feeding the follow-up input into the previous model, one of the following two cases could happen. First, the inference on follow-up input is not “mouse” anymore. It indicates that the inference on the source input is not based on the object(*mouse*)-relevant features. Since the object *mouse* is still in the

input, if the inference on the source input is based on the object(*mouse*)-relevant features, the inference should still be the “mouse”. Second, the inference on follow-up input remains the same label. It implies that the inference on the source input is based on the object(*mouse*)-relevant features. When the object-relevant features are preserved, the model can leverage them to make the correct inference. Such a situation is in line with human expectations. Motivated by this example, we propose the following MR-2. In the above example, MR-2 is violated in the first situation and satisfied in the second situation.

MR-2 An image mutated by preserving the features of the target object(s) and corrupting other features should lead to an inference result with the same label(s).

Relation Formulation of MR-2 Let i'_p be a follow-up input constructed from a source input i for a model \mathcal{M} by preserving the target object(s) but mutating the other parts. We consider such a mutation *object-preserving*. An example of object-preserving mutation is shown in Figure 1a (source input) and Figure 1c (follow-up input). MR-2 mandates that $\mathcal{M}(i)$ and $\mathcal{M}(i'_p)$ should satisfy the relation: $\mathcal{D}(\mathcal{M}(i), \mathcal{M}(i'_p)) \leq \Delta_p$. Here, Δ_p denotes a threshold for the distance between two inference results made by a model under metamorphic testing using object-preserving mutations. The detailed definition of D for MR-2 is introduced in Section 4.4.2.

Explanation of MR-2 If an inference made by a specific model is based on object-relevant features, after object-preserving mutations, the labels of the new inference result should not be changed, since the object-relevant features are preserved and the model should be able to use them.

4 Approach

We present our approach in this section, starting from an overview of the whole approach, followed by the explanation of each stage.

4.1 Overview

Figure 3 shows the overview of our approach, including the following three stages:

① **Object-Relevant Feature Identification** Given an inference to be examined, we regard its input image as the source input. We semantically divide the input into two parts, a *target-object region* and a *background region*. The *target-object region* is where the target object(s) is located and where the object-relevant features are encoded. The *background region* is where the object-irrelevant features are encoded.

② **Follow-up Inputs Construction** Mutation functions are leveraged to generate follow-up inputs from the source inputs, based on the proposed metamorphic relations. Specifically, these mutation functions will corrupt, or preserve the object-relevant features in the source input. The corresponding testing oracles will also be generated based on the metamorphic relations.

③ **Metamorphic Relation Validation** We validate if the distance between the inference result of a source input and the inferences of its follow-up inputs violates the test oracles. If so, the inference of the source input is flagged as an

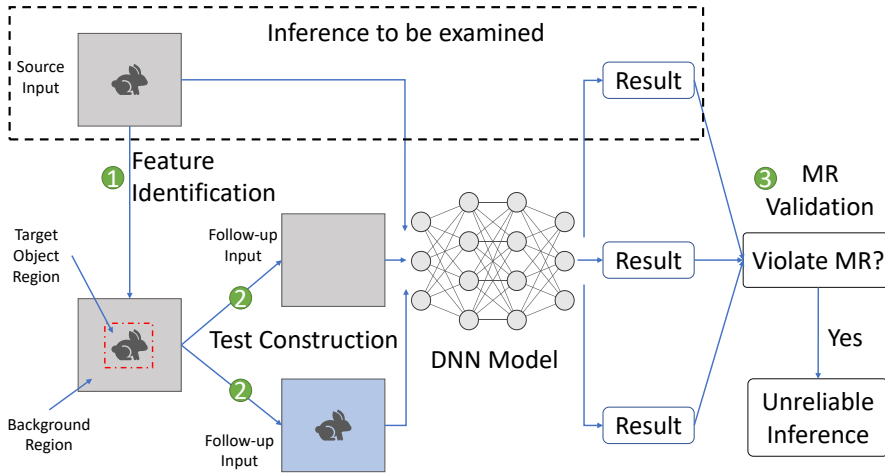


Fig. 3: The Overview of our Metamorphic Testing Approach

341 *unreliable inference*, which means this inference is made mainly based on object-
 342 irrelevant features.

343 Please note that our approach mainly assesses the correct inference results
 344 from image classification models. In single-label classification, “correct” means
 345 that the top-1 label in the result is the same as the source input’s ground truth.
 346 In multi-label classification, “correct” means that the set of labels in the results is
 347 the same as the set of labels in the source input’s ground truth, as we mentioned in
 348 Section 2.2. We focus on correct inferences since if the inference result is incorrect,
 349 the target object might not exist in the input, and thus it is challenging to identify
 350 the object-relevant features.

351 4.2 Object-Relevant Feature Identification

352 In single-label classification, since each image only has a single label, we regard
 353 the object(s) belonging to the annotated label as the target object(s). For multi-
 354 label classification, each image can have multiple labels. We regard the union of
 355 all objects belonging to the annotated labels as the target objects. For example,
 356 for the input as shown in Figure 2c, the target objects consist of the airplane,
 357 motorcycle and person. In both cases, the pixels where the target object(s) reside
 358 are treated as the *target-object region* and the others are regarded as the *background*
 359 *region*.

360 The annotations of the target objects could be extracted from the dataset, or
 361 obtained using the latest object localization techniques, such as YOLO (Redmon
 362 et al. 2016) and Faster R-CNN (Ren et al. 2017). Currently, several datasets for
 363 image classification provide the annotation of objects, such as ImageNet, COCO,
 364 PASCAL VOC and Google Open Image. The annotations are usually in the format
 365 of a *bounding box*. For example, the bounding box of the *tiger shark* in Figure 2a is

366 displayed as the red rectangle in Figure 2b. Some datasets, such as COCO, anno-
367 tate the object using the object mask, which draws the boundary of each object
368 with a finer granularity. These annotations provide the exact target-object region
369 that does not contain any pixels belonging to the background region. Figure 2d
370 shows the object marks of “person”, “motorcycle” and “airplane”.

371 Both annotation formats can be used in our approach. If the annotations are
372 provided as bounding boxes, we regard the region of the bounding boxes as the
373 target-object region. Although the target-object region could contain some pixels
374 that do not belong to the target object(s), the majority of the region represents the
375 target object. If the annotations are object masks, we regard the region covered
376 by the object masks as the target-object region. In our experiment, we used the
377 bounding box for the experiments based on the ImageNet dataset and the object
378 mask on the COCO dataset, depending on the availability of the annotation format
379 in these datasets.

380 4.3 Follow-up Inputs Construction

381 We generate the follow-up inputs by semantically corrupting or preserving the
382 object-relevant features of a source image using the two aforementioned image
383 mutations: *object-corrupting* mutation and *object-preserving* mutation.

384 There are many possible ways to design the mutation functions to corrupt or
385 preserve the object-relevant features. However, it is challenging to quantitatively
386 measure the degree of corruption and preservation. Such a challenge further brings
387 difficulties to define the test oracle, as different levels of corruption and preserva-
388 tion should correspond to different designs of test oracle, especially the thresholds
389 of test oracle (e.g., the Δ_c in Section 3). An inappropriate test oracle will influence
390 the effectiveness of our approach.

391 To alleviate this challenge, we mutate the image by filling simple colors, such
392 as white, gray and black, into the target-object region (or background region).
393 Correspondingly, we use whether the classification results of source input and
394 follow-up input are equal as the test oracle. The objective of our mutation is to
395 simulate extreme cases, without considering the realism of images. For example, if
396 the target-object region in the source input is substituted by black color, i.e., the
397 object-relevant features are removed, but the model can still classify it correctly,
398 the model is very likely to make the inference based on the object-irrelevant fea-
399 tures. In real scenarios, our mutation can be considered as the simulation of the
400 blocking of cameras. An existing study (Pei et al. 2017) designed for testing DNNs
401 also generates test images via randomly patching black holes to images, in order
402 to simulate the blocking of cameras.

403 Besides alleviating the above challenge, another advantage of using simple col-
404 ors is that these colors bring little additional features to the source input. If we
405 replace the object region with other objects or patterns, they may bring new fea-
406 tures and further affect the model inference results. In such a situation, one cannot
407 easily identify whether the change of the inference result is due to the absence of
408 object-relevant features, or the appearance of these new features.

409 In our experiments, we use three colors, i.e., black (R0, G0, B0), gray (R127,
410 G127, B127) and white (R255, G255, B255). For each source input, three follow-
411 up inputs are generated based on MR-1 and three more are generated based on

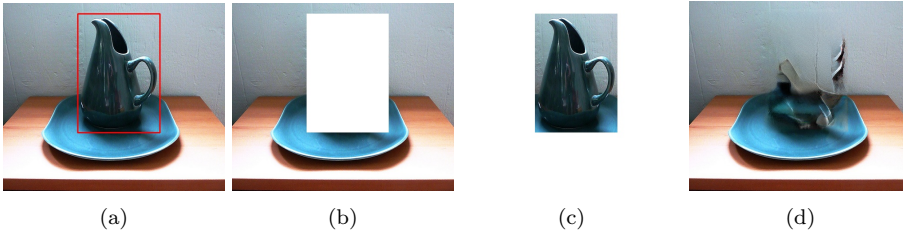


Fig. 4: (a): Original Image with Bounding Box, Label: “pitcher, ewer”. (b): Image after Object Corrupting Mutation for MR-1. (c): Image after Object Preserving Mutation for MR-2. (d): Image Inpainting Result using DeepFill.

412 MR-2. For example, given the source input shown in Figure 4a, Figure 4b and
 413 Figure 4c are two follow-up inputs generated based MR-1 and MR-2, respectively.
 414 It is possible that such simple colors could also induce bias to model inference. To
 415 alleviate this threat, eventually, we use the majority of their validation results as
 416 the final result. Such a strategy is called the *majority voting* (Freund and Schapire
 417 1995) and it has been used by an existing study (Pei et al. 2017) to test DNN
 418 systems. One threat to validity that might be raised is whether three colors are
 419 sufficient for performing metamorphic testing. To alleviate this threat, we compare
 420 the results using more colors in Section 5.2, and demonstrate that using three colors
 421 is sufficient.

422 Another threat that might be raised is why not using the inpainting technology
 423 to remove the object/background more naturally. Actually, we tried this method
 424 at the exploratory stage of this study. However, even the-state-of-art technology
 425 DeepFill (Yu et al. 2018) cannot completely remove the object features. An exam-
 426 ple is shown in Figure 4d. The feature of pitcher in the image cannot be removed
 427 completely. Moreover, such inpainting models usually need hundreds of hours for
 428 training and ~ 15 seconds to inpaint an image, which is not efficient.

429 4.4 Metamorphic Relation Validation

430 In this subsection, we introduce the metamorphic relation validation process.
 431 Please note that in our experiments on single-label and multi-label classification
 432 models, for each source input i , we generate three follow-up inputs i' s. Then we
 433 will validate the MRs three times and use majority voting to decide whether MRs
 434 are violated. As we mentioned, such a method can mitigate the possible threat
 435 induced by a single mutation. We will regard $\mathcal{M}(i)$ as an unreliable inference if
 436 and only if MR-1 is violated at least two out of three times. The same strategy is
 437 applied for MR-2.

438 4.4.1 Validation of MR-1

439 **MR-1** An image mutated by corrupting only the features of the target object(s)
 440 should lead to an inference result with different label(s), or an inference result
 441 with the same label(s) but less certainty.

Single-label Classification Here we use the same notation as Section 3. We define the distance function \mathcal{D} as follows:

$$\mathcal{D}(\mathcal{M}(i), \mathcal{M}(i'_c)) = \begin{cases} 1, & \text{if } l_{\mathcal{M}(i)} \neq l_{\mathcal{M}(i'_c)} \\ & \text{or if } l_{\mathcal{M}(i)} = l_{\mathcal{M}(i'_c)} \text{ and } \mathcal{C}(l_{\mathcal{M}(i)}) > \mathcal{C}(l_{\mathcal{M}(i'_c)}) \\ 0, & \text{otherwise} \end{cases}$$

Here, $l_{\mathcal{M}(i)}$ is the label of the target object in $\mathcal{M}(i)$. $\mathcal{C}(\mathcal{M}(i))$ measures the certainty of the $\mathcal{M}(i)$, according to the definition proposed by existing work in DNN testing (Xie et al. 2019b; Zhang et al. 2020b):¹

$$\mathcal{C}(\mathcal{M}(i)) = \min_{0 < j < n, j \neq l} |p_l - p_j|$$

where p_l is the probability of label $l_{\mathcal{M}(i)}$ and p_j is the probability of j -th label in the inference. Intuitively, the certainty measures the minimal difference between label $l_{\mathcal{M}(i)}$ and any other labels in terms of their probabilities. The value of $\mathcal{C}(\mathcal{M}(i))$ ranges in the region $[0, 1]$. The higher the value is, the more certain the model is on the inference. If the inference is a correct inference, the above certainty equation actually calculates the difference between the highest probability and the second highest probability.

Correspondingly, we define Δ_c equals to 1. if $\mathcal{D}(\mathcal{M}(i), \mathcal{M}(i'_c)) \geq \Delta_c = 1$, i.e., the label of the inference on the source input $l_{\mathcal{M}(i)}$ is different from the one of the inference on the follow-up input $l_{\mathcal{M}(i'_c)}$, or the labels are the same but the inference on the follow-up input become less certain, the MR-1 is satisfied. Otherwise, if $\mathcal{D}(\mathcal{M}(i), \mathcal{M}(i'_c)) < \Delta_c = 1$, i.e., $l_{\mathcal{M}(i)}$ and $l_{\mathcal{M}(i'_c)}$ are the same and the certainty increases, it implies that after corrupting the object-relevant features in the source input, the model can still correctly classify the input with more certainty. In other words, the examined inference $\mathcal{M}(i)$ is made based on features irrelevant to the objects. This conclusion violates our MR-1, and thus $\mathcal{M}(i)$ is labeled as an unreliable inference.

Multi-label Classification In multi-label classification, we adapt the above formula with slight modifications to cooperate with the multiple labels. Specifically, we use $L_{\mathcal{M}(i)}$ to denote the set of labels outputted by the model \mathcal{M} on input i . We define the distance function \mathcal{D} as follows:

$$\mathcal{D}(\mathcal{M}(i), \mathcal{M}(i'_c)) = \begin{cases} 1, & \text{if } L_{\mathcal{M}(i)} \neq L_{\mathcal{M}(i'_c)} \\ & \text{or if } L_{\mathcal{M}(i)} = L_{\mathcal{M}(i'_c)} \text{ and } \mathcal{C}(L_{\mathcal{M}(i)}) > \mathcal{C}(L_{\mathcal{M}(i'_c)}) \\ 0, & \text{otherwise} \end{cases}$$

To the best of our knowledge, the certainty in multi-label classification has not been defined by existing work, and the definition in single-label classification cannot be applied to multi-label classification directly. As we introduced in Section 2, in single-label classification, the sum of the probability of all labels is equal to 1. Labels are competing with each other and only the label with the highest probability is regarded as the final result. In other words, the increase of the probability of a label means the decrease of the probability of other labels. Thus, we can measure the certainty based on to what extent the probability of this label is different from the probabilities of the remaining labels. However, as we mentioned

¹ The latter study refers this concept as ‘‘prediction confidence’’

468 in Section 2.2, in multi-label classification, the probabilities of labels are relatively
 469 independent, i.e., the sum of the probabilities of all labels are not necessarily equal
 470 to 1. The difference between the probabilities of the two labels does not imply the
 471 inference certainty.

472 To address this challenge, in our approach, we regard the multi-label classi-
 473 fication into multiple binary-classification tasks where each binary-classification
 474 predicts whether the input belongs to a single label or not. This enables us to
 475 measure the certainty of each label individually. For example, let us assume an
 476 inference result given by a multi-label classification is $[0.8, 0.9, 0.2]$, which corre-
 477 sponds to the probability of “airplane”, “person” and “motorcycle”. We can regard
 478 it as the outputs from three binary-classification models. The first model predicts
 479 whether the input belongs to label “airplane” and outputs the probability 0.8.
 480 The second and third ones predict whether the input belongs to label “person”
 481 and “motorcycle”, and output the probability 0.9 and 0.2, respectively. It is trivial
 482 to calculate the certainty of the binary classification task. Therefore, we can first
 483 measure the certainty of each binary classification, and then leverage the results
 484 to measure the certainty of multi-label classification.

More specifically, for any label l in the inference result of $\mathcal{M}(i)$ and its proba-
 bility p , we define the certainty $\mathcal{C}_{l, \mathcal{M}(i)}$:

$$\mathcal{C}_{l, \mathcal{M}(i)} = |p - (1 - p)| = |2p - 1|$$

485 The value of $\mathcal{C}_{l, \mathcal{M}(i)}$ is within the region $[0, 1]$. The intuition is to measure the
 486 certainty based on the difference between the probability that “it belongs to label
 487 l ” and “it does not belong to label l ”. The larger the difference is, more certain the
 488 model is on the inference. Based on the above definition of certainty of single label
 489 in the multiple-classification, we define the comparison of $\mathcal{C}(L_{\mathcal{M}(i)})$ and $\mathcal{C}(L_{\mathcal{M}(i'_c)})$
 490 as following: $\mathcal{C}(L_{\mathcal{M}(i)}) > \mathcal{C}(L_{\mathcal{M}(i'_c)}) \iff \mathcal{C}_{l, \mathcal{M}(i)} > \mathcal{C}_{l, \mathcal{M}(i'_c)}, \forall l \in L_{\mathcal{M}(i)}$. The
 491 above equation compares the certainty of each label in the inferences on the source
 492 input and the follow-up input. Please note that for the predicate of certainty
 493 $\mathcal{C}(L_{\mathcal{M}(i)})$ and $\mathcal{C}(L_{\mathcal{M}(i'_c)})$, we check it only if the prior predicate $L_{\mathcal{M}(i)} = L_{\mathcal{M}(i'_c)}$
 494 is true.

495 For Δ_c , we use the same definition as single-label classification, i.e., $\Delta_c = 1$. If
 496 $\mathcal{D}(\mathcal{M}(i), \mathcal{M}(i'_c)) \geq \Delta_c$, the MR-1 is satisfied. Otherwise, MR-1 is violated and the
 497 examined inference, i.e., $\mathcal{M}(i)$, is regarded as an unreliable inference.

4.4.2 Validation of MR-2

499 **MR-2** An image mutated by preserving the features of the target object(s) and
 500 corrupting other features should lead to an inference result with the same label(s).

Single-label Classification We define \mathcal{D} as follows:

$$\mathcal{D}(\mathcal{M}(i), \mathcal{M}(i'_p)) = \begin{cases} 0, & \text{if } l_{\mathcal{M}(i)} = l_{\mathcal{M}(i'_p)} \\ 1, & \text{otherwise} \end{cases}$$

501 Here, $l_{\mathcal{M}(i)}$ is the label with the highest probability in $\mathcal{M}(i)$. We define the thresh-
 502 old $\Delta_p = 0$. If $\mathcal{D}(\mathcal{M}(i), \mathcal{M}(i'_p)) > \Delta_p = 0$, it means that the label of the inference
 503 on the source input $l_{\mathcal{M}(i)}$ is different from the one of the inference on the follow-
 504 up input $l_{\mathcal{M}(i'_p)}$. In other words, after preserving the features of the target object

505 and corrupting the remaining features in the source input, the model classifies
 506 the follow-up input into a different label. This conclusion is opposite to our MR-
 507 2, and thus the examined inference $\mathcal{M}(i)$ is labeled as an unreliable inference. If
 508 $\mathcal{D}(\mathcal{M}(i), \mathcal{M}(i'_p)) \leq \Delta_p = 0$, it implies that after preserving the features of the
 509 target object and corrupting the others, the model still classifies the input into
 510 the same label as the one of the source input. This result is in line with our MR-2
 511 and thus the examined inference will not be labeled as an unreliable inference by
 512 us.

Multi-label Classification We define \mathcal{D} as follows:

$$\mathcal{D}(\mathcal{M}(i), \mathcal{M}(i'_p)) = \begin{cases} 0, & \text{if } L_{\mathcal{M}(i)} = L_{\mathcal{M}(i'_p)} \\ 1, & \text{otherwise} \end{cases}$$

513 Here, $L_{\mathcal{M}(i)}$ is the set of labels in $\mathcal{M}(i)$. The equality of the $L_{\mathcal{M}(i)}$ and $L_{\mathcal{M}(i'_p)}$ is
 514 based on the equality of set. In other words, $L_{\mathcal{M}(i)} = L_{\mathcal{M}(i'_p)}$ if and only if for any
 515 element in $L_{\mathcal{M}(i)}$, this element is also in $L_{\mathcal{M}(i'_p)}$ and for any element in $L_{\mathcal{M}(i'_p)}$, it
 516 is also in $L_{\mathcal{M}(i)}$.

517 Same as single-label classification, the Δ_p is defined as 0. If $\mathcal{D}(\mathcal{M}(i), \mathcal{M}(i'_p)) >$
 518 $\Delta_p = 0$, it means $L_{\mathcal{M}(i)}$ and $L_{\mathcal{M}(i'_p)}$ are different. In other words, after preserving
 519 the features of the target object and corrupting the remaining features in the source
 520 input, the model classifies the input into different labels with the inference on the
 521 source input. This conclusion is opposite to our MR-2, and thus the examined
 522 inference $\mathcal{M}(i)$ is labeled as an unreliable inference.

523 5 Evaluation

524 In this section, we evaluate our approach from the perspective of effectiveness.
 525 First, we investigate the effectiveness of our proposed approach to see whether
 526 it can successfully identify inferences that are made based on object-irrelevant
 527 features. Specifically, we measure the precision (true positive rate) of our approach,
 528 i.e., the number of real unreliable inferences in all inferences identified by our
 529 approach. We aim to answer the following question:

530 **RQ1** What is the effectiveness of our approach in terms of true positive rate?

531 Further, as mentioned in Section 4, we use three colors to mutate inputs in our
 532 approach. One threat of our approach is that whether more colors should be used
 533 to identify unreliable inferences. To answer this question, we performed another
 534 experiment in which we use 15 distinct colors to mutate the inputs, and then
 535 compared it with the experiment in which only 3 colors are used. These results
 536 will help us to answer the following question:

537 **RQ2** Is it sufficient to use only 3 colors for mutations in terms of effectiveness?

538 The source code and data of our experiment are available online.² Our ex-
 539 periments were conducted on two datasets, the ImageNet 2012 validation set and
 540 COCO 2014 validation set. The ImageNet 2012 validation set is a popular single-
 541 label classification dataset with 50,000 images. These images evenly distribute
 542 across 1,000 labels. The COCO 2014 validation set is a common multi-label clas-
 543 sification dataset, with 40,504 images across 80 labels. On average, each image
 544 has 7.21 labels. We chose these datasets for three reasons. First, both are popular

² <https://github.com/yqtianust/PaperUnreliableInference>

545 image classification datasets on which most state-of-the-art models are trained.
546 Second, there are plenty of pre-trained models available as experiment subjects.
547 Third, they provide the annotation of object boundaries.

548 5.1 Effectiveness of Our Approach

549 In order to evaluate whether our metamorphic testing approach can effectively
550 identify unreliable inferences, we applied it to the inferences made by three pre-
551 trained single-label classification models from the Keras Application (Chollet et al.
552 2015a) and one multi-label classification model (Ben-Baruch et al. 2020). The
553 former models are trained on the ImageNet dataset and the latter one is trained on
554 the COCO dataset. Then we manually validated the testing results and measured
555 the precision.

556 To validate whether the unreliable inferences identified by our approach are
557 indeed made based on object-irrelevant features, for each of them, we manually
558 checked the quality of their follow-up inputs. If the follow-up inputs are con-
559 structed as expected, i.e., the object features in the follow-up inputs are cor-
560 rupted(preserved) for MR-1(MR-2), we regarded the corresponding inference as
561 indeed unreliable, i.e., a true positive case. If the follow-up inputs are not con-
562 structed as expected, the corresponding inference cannot be regarded as an unre-
563 liable inference, thus resulting in a false positive case.

564 More specifically, for the inference results that violate MR-1, we manually
565 checked whether the object-relevant features were completely corrupted after the
566 mutation, i.e., whether the target objects in the follow-up inputs are indeed re-
567 moved. If the follow-up input does not contain the target object, the inference
568 violates MR-1 since the model still predicts it as the original label. Thus, this
569 test result is a true positive. If the follow-up input still contains the target object,
570 predicting it as the original label does not violate MR-1, and hence the identified
571 unreliable inference is a false positive.

572 Similarly, for the inference that violated the relation MR-2, we manually checked
573 whether the target objects were preserved and whether the other features were cor-
574 rupted. Specifically, if the follow-up input contains the target object, the MR-2 is
575 violated since the model does not predict the follow-up input as the original label.
576 So, we labeled the test result as true positive. On the contrary, if the follow-up
577 input does not contain the target object, MR-2 is not violated and the identified
578 unreliable inference is a false positive.

579 The manual check was conducted by two graduate students individually and in-
580 dependently. Only the results agreed by consensus were considered. The disagreed
581 results were labeled as “uncertain”.

582 5.1.1 Pilot Study

583 Before the manual check, we first conducted a pilot study to help us understand the
584 possible cases (i.e., the root cause of false positive cases) that might be encountered
585 in the manual check. Specifically, we randomly selected 200 unreliable inferences
586 found by our approach to perform the pilot study, among which 100 violate MR-1
587 and the others violate MR-2. We investigated whether each unreliable inference is
588 true positive and if not, what are the major reasons for those false positive cases.

589 In the investigation, for each unreliable inference, each student was requested
590 to view a pair of inputs (pictures in our scenarios). More specifically, each pair of
591 the inputs consisted of two inputs: (a) the source input on which the unreliable
592 inference is made, e.g., Figure 4a, and (b) the follow-up input constructed based
593 on the source input, e.g., Figure 4b if MR-1 is violated, or Figure 4c if MR-2
594 is violated. Besides, the label of the source input was provided to the students.
595 The students were required to answer the following questions for the unreliable
596 inferences violating MR-1:

- 597 1. Do you think the object-relevant features of the source input have been com-
598 pletely corrupted in the follow-up inputs, i.e., the target objects in the follow-up
599 inputs have been indeed removed?
- 600 2. If not, please briefly explain the reason.

601 Similarly, for the unreliable inferences violating MR-2, the corresponding ques-
602 tions were:

- 603 1. Do you think the object-relevant features of the source input have been com-
604 pletely preserved in the follow-up inputs, i.e., the target objects still remain in
605 the follow-up inputs?
- 606 2. If not, please briefly explain the reason.

607 First, two graduate students investigated the selected 200 image pairs indi-
608 vidually and independently. Their answers to the questions have been recorded.
609 Then for the inconsistent answers, they discussed with each other to see if they
610 can reach a consensus. A reason is selected as a common reason if it occurs more
611 than or equal to 10 times. Eventually, we finalized three common reasons inducing
612 false positives for unreliable inference violating MR-1, which are:

613 (a)*Existence of Multiple Target Objects*. These false positives occurred because
614 there are multiple target objects in the source input, but not all of them are cor-
615 rupted in the follow-up inputs. Figure 5f shows an example. The original image in
616 Figure 5b, whose label is “confectionery”, has multiple confectioneries. Ideally, all
617 of them should be corrupted in its follow-up inputs. However, after mutation, the
618 follow-up input, as shown in Figure 5f, still contains multiple confectioneries since
619 the dataset only annotates one of them, which is shown as the red rectangle in
620 Figure 5b. As such, the inference of the follow-up input can still be “confectionery”
621 as the object-relevant features (the other confectioneries) are not completely cor-
622 rupted. Therefore, MR-1 is not violated and the original inference is a false positive
623 of the identified unreliable inferences.

624 (b)*Incomplete Removal of the Target Object*. Some false positives occurred in the
625 inputs that contain a single target object but only parts of it are corrupted in
626 the follow-up input. An example is shown in Figure 5c, whose label is “drilling
627 platform”. Ideally, the entire platform should be corrupted in the follow-up inputs.
628 However, the mutated images shown in Figure 5g still contain part of the target
629 object. This is because the annotation provided by the ImageNet dataset does not
630 cover the upper-half of “drilling platform”, which differs from the other images in
631 this label whose platforms are entirely annotated. Therefore, the follow-up input
632 can lead to the same classification result as the original inference because the
633 object-relevant features are not corrupted entirely. The MR-1 is not violated in
634 this case.

635 (c) *Others*. It refers to the other reasons not belonging to the above two reasons.
 636 For example, the original image is not clear and hinders the students to identify
 637 the boundary of the target object.

638 For MR-2, we do not distinguish the reason for false positives since the number
 639 of false positives is very limited (less than 10 in our pilot study).

640 We also conducted a similar pilot study for multi-label classification. More
 641 specifically, we selected 50 unreliable inferences violating MR-1 and 50 ones vio-
 642 lating MR-2 from all the unreliable inferences in multi-label classification found by
 643 our approach. A reason is considered common if it occurs at least 5 times. Since
 644 we did not notice other reasons than the ones aforementioned, we concluded the
 645 same reasons for both single-label and multi-label classifications.

646 5.1.2 Experiment Setup

647 **Model Selection** For the single-label classification model, we selected NASNet-
 648 Large (Zoph et al. 2018), MobileNet (Howard et al. 2017) and ResNet101 (He
 649 et al. 2016) among the pre-trained models from the Keras Application (Chollet
 650 et al. 2015b) because their top-1 accuracy lies at the top, medium and bottom,
 651 respectively, among those of the models. For the multi-label classification model,
 652 we selected TResNet-XL (Ben-Baruch et al. 2020), since it achieves the highest
 653 accuracy on the COCO dataset to the best of our knowledge (Ben-Baruch et al.
 654 2020) till March 2021.

655 **Sampling** We randomly sampled the inferences made by the four models
 656 for the manual check, where the sample size is determined by the Cochran for-
 657 mula (Cochran 1963) with 95% confidence level.

658 **Manual Check** Two graduate students conducted the manual check similar to
 659 the pilot study. More specifically, each source input in the unreliable inference was
 660 displayed with the follow-up inputs constructed by our method. The students were
 661 asked the same question as the ones in the pilot study. The only difference is that
 662 at this time, the Q2 in unreliable inference violating MR-1 was supplied with three
 663 options, which are: (a) *Existence of Multiple Target Objects*, (b) *Incomplete Removal*
 664 *of The Target Object*, (c) *Others*. When (c) is chosen, the students were also required
 665 to write down detailed explanations. The students were allowed to choose multiple
 666 of the above options. During the manual check, we also monitored the reasons in
 667 (c) *Others*. If any reason in (c) *Others* occurs at least 10 times, we would extract
 668 a new common reason. Such a situation does not exist in our manual check.

669 Each student conducted the manual check individually and independently. It
 670 took around 15 hours for each of them to complete the manual check. After the
 671 individual check, they discussed the cases where the disagreement arises, in case
 672 any of them miss anything during the check. If the disagreement is addressed, the
 673 corresponding manual check result is changed. At last, we collected and analyzed
 674 the results. As we mentioned previously, only the results agreed by consensus were
 675 considered in the analysis. The Kappa Agreement Score (Landis and Koch 1977)
 676 of the manual check is 0.955. Such a value indicates an almost perfect agreement
 677 between the two graduate students who conducted the manual check.

678 **Threat to validity** There is a potential threat to validity in this experiment.
 679 Our manual check is subject to human mistakes. To address the threat, two gradu-
 680 ate students conducted the manual check individually and independently. A result



Fig. 5: (a)(b)(c)(d): Images (with Bounding Boxes) as the Source Inputs. (e)(f)(g)(h): Images as the Corresponding Follow-up Inputs. Labels: (a): “goldfinch, *Carduelis carduelis*”, (b): “confectionery”, (c): “drilling platform”, (d): “car wheel”.

Table 1: The Manual Check Results for the Effectiveness of MR-1 on Single-label Classification Models. Column *Multiple* is for the Reason *Existence of Multiple Target Objects* and Column *Incomplete* is for the Reason *Incomplete Removal of the Target Object*. The Number in the Parentheses under *Multiple* is for Cases Shared by Both Reasons.

Model	Accuracy	Total	Sample Size	True Positive	False Positive			Uncertain
					Multiple	Incomplete	Others	
NASNetLarge	82.7%	826	311	202 (65.0%)	84 (1)	16	4	6
ResNet101	76.4%	344	194	122 (62.9%)	55 (2)	8	8	3
MobileNet	70.3%	222	149	95 (63.8%)	42 (1)	8	3	2
Total		1,392	654	419 (64.1%)	181 (27.7%)	32 (4.9%)	15	11

681 will be adopted only if both students made the same conclusion. The high Kappa
682 Agreement Score indicates that the results is reliable.

683 5.1.3 Results and Discussion

684 **Single-label Classification Models** Table 1 and Table 2 show the manual check
685 results for MR-1 and MR-2 for single-label classification models, respectively. The
686 column *Total* refers to the number of unreliable inferences identified by our ap-
687 proach for each model. Specifically, our approach identifies 1,392 inferences that
688 violate MR-1 and 15,198 inferences that violate MR-2. We randomly sampled and
689 manually checked 654 and 1,069 inferences from these two categories, respectively,
690 as previously explained.

Table 2: The Manual Check Results for the Effectiveness of MR-2 on Single-label Classification Models.

Model	Accuracy	Total	Sample Size	True Positive	False Positive	Uncertain
NASNetLarge	82.7%	3,634	348	339 (97.4%)	1	8
ResNet101	76.4%	4,942	357	340 (95.2%)	7	10
MobileNet	70.3%	6,622	364	351 (96.4%)	0	16
Total		15,198	1,069	1,030 (96.4%)	8(0.07%)	34

Table 3: The Manual Check Results for the Effectiveness of MR-1 and MR-2 on Multi-label Classification Model: TResNet-XL).

MR	Total	Sample Size	True Positive	False Positive	Uncertain
MR-1	957	275	215 (78.2%)	44	16
MR-2	4,732	356	308 (86.5%)	30	18

691 As for the inputs that violate MR-1, the column *True Positive* of Table 1 shows
692 that our approach achieves an average precision of 64.1%, ranging from 62.9% to
693 65.0% for different models. Out of the 654 samples, 419 samples do not contain
694 the target objects in the follow-up inputs but the models keep labeling them as
695 the target objects. So, they violate MR-1 and are true positive cases. Figure 5a
696 shows an example, in which the original image is correctly classified by the model
697 ResNet101 as “goldfinch, *Carduelis carduelis*”. Although the follow-up input in
698 Figure 5e does not contain birds, ResNet101 gives the same classification result as
699 that of the original image, thus resulting in an unreliable inference.

700 We further checked the remaining 235 (=654 - 419) false positive cases, and
701 found that 77.0% (=181/235) of the false positive cases are due to the *Existence*
702 *of Multiple Target Objects* and 13.6%(=32/235) are because of *Incomplete Removal*
703 *of the Target Object*. Moreover, there are four cases that belong to both *Existence*
704 *of Multiple Target Objects* and *Incomplete Removal of the Target Object*. The above
705 numbers (181 and 32) have included these four cases. Besides, there are 11 cases
706 labeled as uncertain as the results from two students disagree with each other.
707 The rest of the false positive cases (15 in total) are labeled as Others.

708 As for the inputs that violate MR-2, it shows that our approach achieves an
709 aggregated precision of 96.4%, ranging from 95.2% to 97.4% for different models.
710 In total, 1,030 out of the 1,069 samples preserve the target objects in the follow-up
711 inputs, but these follow-up inputs are not correctly classified by the models. There-
712 fore, these samples indeed violate MR-2 and they are regarded as true positives of
713 the unreliable inferences violating MR-2. For the remaining 39 cases, only part of
714 the target objects is preserved in the follow-up inputs. They do not violate MR-2
715 and are false positives. For instance, given the source input as shown in Figure 5d,
716 the constructed follow-up input in Figure 5h only covers the center of wheel but not
717 the entire tire. According to the definition from the WordNet (Fellbaum 2006) (the
718 labels of the ImageNet dataset are defined according to WordNet), “car wheel”

719 is “a wheel that has a tire and rim and hubcap”. Since the object-relevant features
720 are only partially preserved, it makes sense that the follow-up input is incorrectly
721 classified. Therefore, MR-2 is not violated and this is a false positive case.

722 We noticed that the precision of MR-2 is much higher than that of MR-1. We
723 found the reason is that the aforementioned *Existence of Multiple Target Objects* will
724 cause the follow-up input unqualified for the validation of MR-1, as the object-
725 relevant features of the follow-up inputs will not be completely corrupted. However,
726 such a situation will not affect MR-2 since as long as one of the target objects is
727 preserved in the follow-up inputs, the follow-up inputs are valid to validate MR-2.

728 **Multi-label Classification Models** Table 3 shows the manual check results for
729 MR-1 and MR-2 for TResNet-XL, a multi-label classification model, respectively.
730 The true positive rate for MR-1 and MR-2 is 78.2% and 86.5% respectively. This
731 shows that our approach is also effective for multi-label classification models. As
732 for the false positives for MR-1, the major reasons are still *Existence of Multiple*
733 *Target Objects* and *Incomplete Removal of The Target Object*. They account for 20
734 and 23 of the 44 false positive cases. The remaining one is due to the incorrect
735 annotation, where a labeled broccoli is actually lettuce. For the false positives for
736 MR-2, similar to single-label classification, the major reason is that their target
737 objects are not completely preserved in the follow-up inputs and thus they do not
738 violate MR-2.

739 **Answer to RQ1** Our approach is effective in identifying unreliable inferences
740 that violate MR-1 and MR-2, with an aggregated precision of at least 62.9% and
741 86.5%, respectively. The false positives are mainly caused by imperfect annotation
742 of the target objects.

743 5.2 The Impact of The Number of Colors in Our Approach

744 As mentioned in Section 4, we use three colors to mutate inputs in our approach
745 and use the majority of their results to identify the unreliable inference. One threat
746 of our approach is that whether three colors are sufficient to identify unreliable
747 inferences. To answer this question, we performed another experiment that uses 15
748 distinct colors to mutate the inputs, and we then compared the results obtained
749 of the new experiment with that of the original one.

750 5.2.1 Experiment Design

751 Specifically, besides the three colors we used previously, we select 12 more com-
752 monly used colors, which are red (R255, G0, B0), maroon (R128, G0, B0), yellow
753 (R255, G255, B0), olive (R128, G128, B0), lime (R0, G255, B0), green (R0, G128,
754 B0), aqua (R0, G255, B255), teal (R0, G128, B128), blue (R0, G0, B255), navy
755 (R0, G0, B128), fuchsia (R255, G0, B255), and purple (R128, G0, B128). We use
756 the same approach as mentioned in Section 4. The only difference is that now we
757 regard an inference as unreliable if and only if the MR is violated by at least 8 out
758 of the 15 mutated inputs.

759 After the data collection, we compared the results using 15 colors and the
760 ones using 3 colors. Statistically, we use the Chi-square independence test (F.R.S.
761 1900) to test the independence of the results obtained from the two approaches.
762 The Chi-square independence test is commonly used to determine if there is a

Table 4: Contingency Tables for MR-1 and MR-2 to Compare the Experiment Results Obtained using 3 Colors vs 15 Colors.

	MR-1		MR-2	
	V_3 : Violate	V_3 : Not Violate	V_3 : Violate	V_3 : Not Violate
V_{15} : Violate	169	52	5,145	1,467
V_{15} : Not Violate	63	35,323	249	28,773

763 significant relationship between two categorical variables. In our experiment, we
 764 use it to determine if the decision “violate MR or not” using by three colors and
 765 the one using fifteen colors are strongly correlated. If yes, we can use three colors
 766 to save computation resources. We conduct the experiment using the pre-trained
 767 VGG16 from Keras.

768 5.2.2 Results and Discussion

769 We use variable V_3 to denote the decision “violate MR or not” according to the
 770 approach using three colors. Similarly, we use variable V_{15} to denote the decision
 771 “violate MR or not” according to the approach using 15 colors. We build the
 772 contingency tables for both MR-1 and MR-2 as shown in Table 4. The cell in the
 773 table represents the number of the inferences identified by the two approaches.
 774 For example, the cell “169” means there are 169 inferences that are considered as
 775 violating MR-1 by both the approach using three colors and the one using fifteen
 776 colors. The cell “1,467” means there are 1,467 inferences that are considered as
 777 not violating MR-2 by the approach using three colors and considered as violating
 778 MR-2 by the approach using the fifteen colors.

779 The p-values of the Chi-square test are both < 0.001 for MR-1 and MR-2,
 780 which is less than the typical threshold 0.05. The corresponding effect sizes³ are
 781 0.743 and 0.835 for MR-1 and MR-2, respectively. It indicates that the results
 782 obtained by the approach using three colors and the approach using fifteen colors
 783 are strongly correlated. In other words, if an inference is considered unreliable (or
 784 reliable) by the approach using three colors, the same decision will likely be made
 785 by the approach using fifteen colors, and vice versa. Overall, this experiment shows
 786 that using more colors than three in our approach has a minor difference compared
 787 to three colors. Therefore, it is sufficient to use three colors for the follow-up input
 788 construction in our approach.

789 **Answer to RQ2** Using three colors in our approach is sufficient to identify
 790 unreliable inputs effectively.

791 6 Empirical Study

792 Leveraging our approach, we conduct an empirical study to understand the unre-
 793 liable inference problems in reality.

794 First, we want to understand the pervasiveness of the problem, i.e., to what
 795 extent are the inference results made by the state-of-the-art DNN models based

³ in the Chi-square test, it is usually referred to as Cramér’s V (Cramer 1946)

on object-irrelevant features. Specifically, we measure the proportion of unreliable inferences identified in all correct inferences outputted by these models.

RQ3 How pervasive is unreliable inference in DNN models?

Second, we study the characteristics of the identified unreliable inferences. Specifically, we focus on the size of the target objects in unreliable inferences, a common attribute of objects. We studied whether there is any correlation between the object size and the unreliable inferences.

RQ4 Is there a correlation between the target object size and the unreliable inferences?

Next, we aim to understand the effect of such unreliable inferences. Specifically, we investigate whether the unreliable inferences can significantly affect a model’s evaluation result, thus preventing us from correctly evaluating models and comparing them fairly. In the experiments, we compare the accuracy of a model before and after removing those unreliable inferences from the associated test.

RQ5 To what extent will the unreliable inference affect a model’s evaluation?

Finally, we investigate how to tame unreliable inferences. Specifically, we investigate whether the ratio of unreliable inferences can be reduced during the training process and whether it is correlated with the evaluation metrics such as accuracy. To achieve this goal, in the experiments, we track the ratio of unreliable inferences and the model accuracy during the model training process .

RQ6 Can the unreliable inference be tamed during training?

6.1 Pervasiveness of Unreliable Inferences

RQ3 How pervasive is unreliable inference in DNN models?

6.1.1 Motivation

In the previous section, we showed that thousands of inferences made by the four pre-trained classification models violate our MRs. In this subsection, we investigate the pervasiveness of the problem, i.e., whether such unreliable inferences generally exist in a wide variety of models with different architectures. We leveraged our methodology to identify the unreliable inferences made by both the single-label and multi-label image classification models. Then we measure the ratio of the unreliable inferences in all correct inferences. This research question can help us to understand the severity of the unreliable inferences.

6.1.2 Experiment Setup

We collected 21 pre-trained DNN models from public repositories. 18 out of the 21 models are single-label image classification models, and they are collected from the Keras Application (Chollet et al. 2015b), a famous and popular repository for pretrained models. All of them are trained on the ImageNet dataset, and their information (name and accuracy) is shown in the first two columns of Table 5. Besides the single-label classification models, we also collected three multi-label classification models, which are ResNet-50 (He et al. 2016), TResNet-L (Ben-Baruch et al. 2020) and TResNet-XL (Ben-Baruch et al. 2020). ResNet-50 is chosen as it has been used as an experiment subject by existing papers (Zhao et al.

2017; Tian et al. 2020b) and the other two models are included because they are the state-of-the-art in terms of accuracy (till March 2021). All three multi-label classification models are trained on the COCO dataset. Please note that the number of public available multi-label classification models is much smaller than that of the single-label classification models, and we have tried our best efforts to collect these three models.

In the experiment, we found that Keras Application only provided the trained model, but missed the source code to reproduce the results for image classification, especially the code to preprocess the input. To avoid the possible mistakes in reproduction, we leveraged the functionality provided by an open-source toolbox, EvalDNN (Tian et al. 2020a), which has successfully reproduced the reported accuracy for most of the 18 models. The maximum difference between the reported accuracy and the reproduced one is only 0.7%, which demonstrates that we have faithfully deployed the models in our experiments. For the multi-label classification models, we successfully reproduced the results by leveraging the detailed source code provided by the authors.⁴ For the threshold in multi-label classification models, we use the value suggested by their documentation, i.e., 0.5 for TResNet-L and TResNet-XL, and 0.7 for ResNet-50. The columns *Reproduced Accuracy* of Table 5 and Table 6 list the accuracy reproduced in this study for single-label classification and multi-label models, respectively. After the deployment, we applied our approach to identify unreliable inferences from all the correct inferences made by these models.

Threats to validity There are two potential threats to validity in this experiment. First, the models used in this experiment may not include all the DNN-based image classification models and our conclusion may have bias. To mitigate the threat, we collected 21 representative and popular models. They covered most of the modern advanced architectures used in image classification. We believe that our conclusions can be generalized. Second, the inference results of these model can be affected due to the mistake in model deployments. To alleviate this threat, we leveraged the existing toolbox (Tian et al. 2020a) and the source code provided by the authors. We ensured that the models deployed in our experiment perform closely to the accuracy reported in their original research publications and documentations.

6.1.3 Results and Discussion

Table 5 and Table 6 show the experimental results of single-label classification models and multi-label classification models, respectively. For each cell, the percentage displayed in the parentheses is the ratio of the number of unreliable inferences found by our approach with respect to the number of the correct inferences. Please note that the column *Inferences Violating MR-1* refers to the number of inferences violating MR-1, regardless of whether MR-2 is violated or not. The column *Inferences Violating MR-2* refers to the number of inferences violating MR-2, regardless of whether MR-1 is violated or not. The last column *Inferences Violating MR-1&2* refers to the number of inferences violating both MR-1 and MR-2.

⁴ TResNet-L: <https://github.com/Alibaba-MIIL/ASL>, ResNet-50: <https://github.com/ARISE-Lab/DeepInspect>

Table 5: Single-Label Image Classification Models, their Accuracy, the Number and Ratio of Unreliable Inferences Violating MRs on the ImageNet dataset.

Model	Reproduced Accuracy	Inferences Violating MR-1	Inferences Violating MR-2	Inferences Violating MR-1&2
Xception	79.0%	374 (0.95%)	4,104 (10.39%)	229 (0.58%)
VGG16	71.3%	259 (0.73%)	5,394 (15.14%)	228 (0.64%)
VGG19	71.3%	252 (0.71%)	5,628 (15.80%)	219 (0.61%)
ResNet50	74.9%	253 (0.68%)	5,248 (14.01%)	197 (0.53%)
ResNet101	76.4%	344 (0.90%)	4,942 (12.93%)	268 (0.70%)
ResNet152	76.6%	334 (0.87%)	4,727 (12.34%)	266 (0.69%)
ResNet50V2	75.3%	247 (0.66%)	5,387 (14.30%)	213 (0.57%)
ResNet101V2	76.9%	271 (0.70%)	4,606 (11.98%)	212 (0.55%)
ResNet152V2	77.7%	319 (0.82%)	4,392 (11.30%)	252 (0.65%)
InceptionV3	77.9%	404 (1.04%)	4,663 (11.98%)	292 (0.75%)
InceptionResNetV2	80.4%	686 (1.71%)	3,998 (9.94%)	388 (0.97%)
MobileNet	70.3%	222 (0.63%)	6,622 (18.83%)	195 (0.55%)
MobileNetV2	71.2%	281 (0.79%)	6,437 (18.08%)	225 (0.63%)
DenseNet121	75.0%	278 (0.74%)	4,349 (11.60%)	219 (0.58%)
DenseNet169	76.2%	340 (0.89%)	4,154 (10.91%)	264 (0.69%)
DenseNet201	77.3%	334 (0.86%)	4,296 (11.11%)	260 (0.67%)
NASNetMobile	73.8%	461 (1.25%)	6,505 (17.64%)	345 (0.94%)
NASNetLarge	82.7%	826 (2.00%)	3,634 (8.79%)	383 (0.93%)

Table 6: Multi-label Image Classification Models, their Accuracy, the Number and Ratio of Unreliable Inferences Violating MRs on the COCO dataset.

Model	Reproduced Accuracy	Inferences Violating MR-1	Inferences Violating MR-2	Inferences Violating MR-1&2
ResNet50	34.5%	657 (4.71%)	4,873 (34.91%)	422 (3.0%)
TResNet-L	45.5%	1,013 (5.49%)	5,028 (27.26%)	442 (2.4%)
TResNet-XL	47.9%	957 (4.93%)	4,732 (24.38%)	362 (1.9%)

881 The results reveal that each selected single-label and multi-label DNN classi-
882 fication model makes hundreds of unreliable inferences violating MR-1 and thou-
883 sands of ones violating MR-2. In terms of ratio, for single-label classification,
884 our approach identifies that 0.63%~2.00% of the correct inferences violate MR-
885 1, and 9.79%~18.83% of the correct inferences violate MR-2. As for multi-label
886 classification, the ratio is much higher. Specifically, our approach identifies that
887 4.71%~5.49% of the correct inferences violate MR-1, and 24.38%~34.91% of the
888 correct inferences violate MR-2. Furthermore, there are around 2% of the infer-
889 ences violating both MR-1 and MR-2. The results show that the phenomenon,

890 i.e., model makes inferences based on object-irrelevant features, generally exists
891 across different models.

892 We further investigated whether different models will make unreliable infer-
893 ences towards different test inputs. If most of the models make unreliable infer-
894 ences for the same set of inputs, it is more likely that these inputs are defective.
895 To conduct the investigation, we studied for each input the number of different
896 models whose inference for the input was unreliable. Specifically, the number of
897 different models varies from 1 to N , where N is the total number of models in-
898 cluded in our experiments. More specifically, N is 18 for single-label classification
899 on the ImageNet dataset and 3 for multi-label classification on the COCO dataset.
900 We then calculated the ratio of inputs, for which unreliable inferences were made
901 by n models ($n = 1, 2, \dots, N$), with respect to the total number of inputs for which
902 unreliable inferences were made by at least one model.

903 Figure 6a and Figure 6b show the results for single-label classification mod-
904 els on the ImageNet dataset and multi-label classification models on the COCO
905 dataset, respectively. It can be observed that, for single-label classification, 43.7%
906 and 31.8% of the inputs concern unreliable inferences violating MR-1 and MR-2
907 made by only one model, respectively. More than half of the inputs concern un-
908 reliable inferences made by three or fewer models. Only a small portion of inputs
909 (less than 2.7%) concern unreliable inferences made by all 18 models. A similar
910 pattern can also be found for multi-label classification models. 74.3% and 67.4% of
911 the inputs concern unreliable inferences violating MR-1 and MR-2 made by only
912 one model, respectively. Less than 7.8% of the concern unreliable inferences made
913 by all three models.

914 Such results reveal that different models make unreliable inferences for different
915 sets of inputs, which indicates that such unreliable inferences are more likely to
916 be caused by the models themselves instead of the inputs.

917 **Answer to RQ3** The problem of making unreliable inferences is common to
918 state-of-the-art models. Since these models make unreliable inferences on different
919 input sets, the problem is likely to be caused by models instead of inputs.

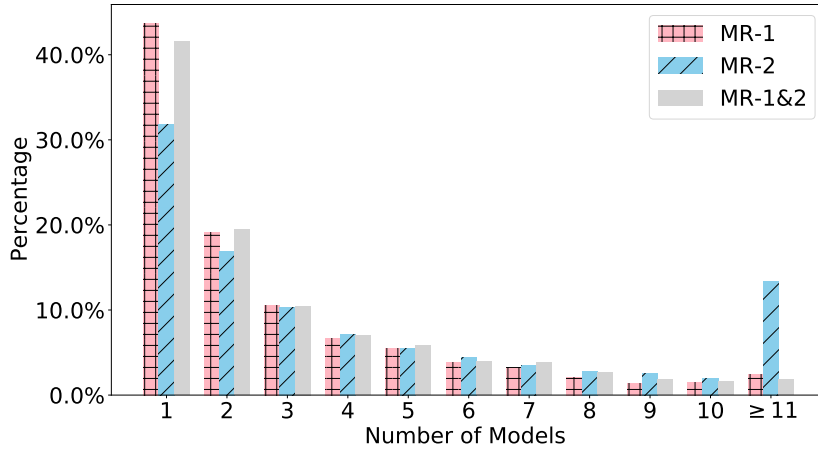
920 6.2 Characteristic of Unreliable Inferences

921 **RQ4** Is there a correlation between the target object size and the unreliable infer-
922 ences?

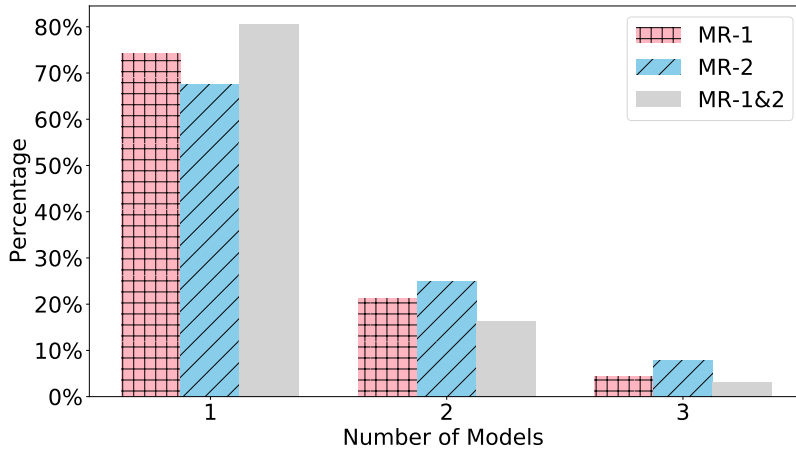
923 6.2.1 Motivation

924 As shown in Section 6.1, unreliable inferences are pervasive, and different models
925 make unreliable inferences for different inputs. We are curious about whether com-
926 mon characteristics exhibit among unreliable inferences. If so, we may give some
927 useful suggestions to developers.

928 We manually investigated those inputs that cause unreliable inferences made
929 by most models. We observed that the sizes of the target objects in these inputs
930 usually occupy a tiny part of the whole image. Figure 7 shows some examples. The
931 objects of these images are different types of balls whose sizes are often small in
932 the images, especially compared to the sports facilities and players. It motivates



(a) Single-Label Classification Models on the ImageNet Dataset



(b) Multi-label Classification Models on the COCO Dataset

Fig. 6: The Percentage of Inputs for which Unreliable Inferences were Made by Different Number of Single-Label and Multi-label Classification Models

933 us to investigate whether the size of an input’s target object is correlated with its
 934 probability of being unreliably inferred by DNN models.

935 6.2.2 Experiment Design

936 To answer this question, for each unreliable inference, we computed the ratio
 937 of the target object’s size with respect to the size of the whole input image.
 938 Then we divided all inferences into 20 intervals based on their ratios, which are



Fig. 7: The Images that Have Small Objects and Are Unreliably Inferred by DNN Models

939 $[0.05 * i, 0.05 * (i + 1))$ and i ranges from 0 to 20. For each interval, we computed
 940 the ratio of unreliable inferences, with respect to the total number of inferences
 941 belonging to this interval. We selected the NASNetLarge and TRResNet-XL as ex-
 942 periment subjects since they achieved the highest top-1 accuracy in all models used
 943 in our experiment for the ImageNet dataset and the COCO dataset, respectively.

944 6.2.3 Results and Discussion

945 Figure 8a and Figure 8b show the results for the model NASNetLarge on the Image-
 946 Net dataset and for the model TRResNet-XL on the COCO dataset, respectively.
 947 Please note that for each interval, we use its middle point as the value in x-axis,
 948 except for the last interval we use the point 1.0. We observed that for these in-
 949 ferences whose target objects are smaller (relative to the size of the image), they
 950 are more likely to be unreliable. Similar results have been observed among the
 951 other models. We suspect that when the model handles an image whose target
 952 object is small, it often extracts features from the background region. Eventually,
 953 it leverages object-irrelevant features to make decisions.

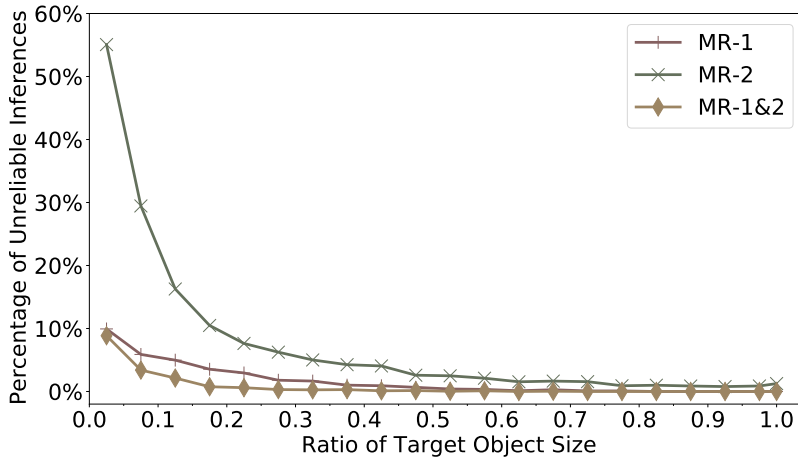
954 **Answer to RQ4** In summary, we found that inputs with small target object
 955 sizes are more likely to be unreliably inferred by existing DNN models. We suggest
 956 the users of these models to pay more attention when making inferences on these
 957 inputs (i.e., the objects' size are less than 30% of the whole image), especially
 958 when deploying these models on safety-critical applications.

959 6.3 Effect of Unreliable Inferences

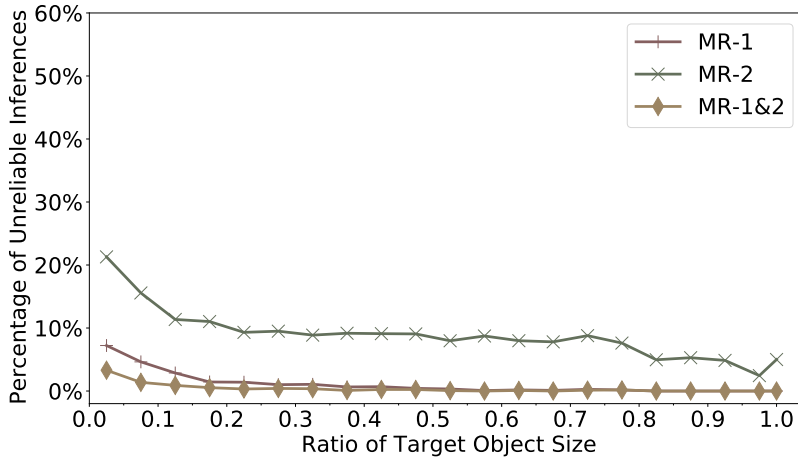
960 **RQ5** To what extent will the unreliable inference affect a model's evaluation?

961 6.3.1 Motivation

962 As revealed by previous sections, a significant proportion of the correct inferences
 963 made by existing models are unreliable. Such pervasiveness of unreliable inferences
 964 might cause bias in understanding and evaluating the performance of different
 965 models. Specifically, if there exists a significant amount of unreliable inferences,
 966 it could induce non-trivial uncertainties in measuring model accuracy. Therefore,



(a) Single-label Classification Model NASNetLarge on the ImageNet Dataset



(b) Multi-label Classification Model TRResNet-XL on the COCO Dataset

Fig. 8: The Ratio of Unreliable Inferences Made by Single-label and Multi-label Classification Models *w.r.t* the Ratio of Target Object Size

967 we investigated the effect of unreliable inferences on model accuracy evaluation in
 968 this experiment.

969 6.3.2 Experiment Design

970 We investigated the effects of unreliable inferences on the measurement of accuracy.
 971 Since both the correct and incorrect inferences can be unreliable and both of them
 972 are important to model evaluations, in this section, we examined both correct and

Table 7: The Comparison of the Top-1 Accuracy between the Unreliable Inferences and Reliable Inferences for Single-label Image Classification Models

Model	Original	MR-1		MR-2		MR-1&2	
		Unreliable	Reliable	Unreliable	Reliable	Unreliable	Reliable
Xception	79.02%	28.22%	80.42%	45.51%	86.40%	20.00%	80.41%
VGG16	71.27%	21.73%	72.48%	41.10%	82.01%	20.07%	72.46%
VGG19	71.26%	20.62%	72.52%	42.21%	81.82%	18.83%	72.50%
ResNet50	74.93%	21.58%	76.21%	44.98%	84.05%	18.17%	76.19%
ResNet101	76.42%	26.34%	77.76%	45.48%	85.01%	22.48%	77.74%
ResNet152	76.60%	26.13%	77.94%	44.88%	85.07%	22.52%	77.91%
ResNet50V2	75.34%	19.92%	76.78%	46.19%	84.21%	17.82%	76.75%
ResNet101V2	76.89%	21.16%	78.37%	45.05%	85.08%	17.76%	78.34%
ResNet152V2	77.73%	23.19%	79.28%	45.51%	85.44%	19.73%	79.25%
InceptionV3	77.87%	30.01%	79.20%	46.05%	85.95%	24.48%	79.17%
InceptionResNetV2	80.41%	42.52%	81.68%	47.43%	87.10%	30.36%	81.73%
MobileNet	70.34%	21.50%	71.38%	42.84%	82.65%	19.52%	71.37%
MobileNetV2	71.19%	23.44%	72.37%	44.47%	82.08%	20.09%	72.36%
DenseNet121	74.97%	22.32%	76.34%	41.89%	83.64%	18.73%	76.32%
DenseNet169	76.18%	26.19%	77.51%	42.02%	84.59%	22.30%	77.48%
DenseNet201	77.32%	26.05%	78.67%	44.60%	85.13%	22.34%	78.63%
NASNetMobile	73.77%	33.12%	74.94%	46.18%	84.60%	27.38%	74.97%
NASNetLarge	82.68%	46.74%	83.99%	49.44%	88.40%	30.25%	84.04%

973 incorrect inferences. For the incorrect inferences, it is possible that they have the
974 labels that do not exist in the ground truth and thus the object-relevant features
975 cannot be directly identified. In such cases, we use the union of all the objects in the
976 annotation to approximate the target object and then identify the object-relevant
977 features.

978 In the investigation, with respect to MR-1, we examined all (both correct and
979 incorrect) inferences and separated them into two sets for each model according
980 to whether they are reliable. One set contains all the inputs whose inferences are
981 identified as unreliable by our approach and another set that contains the remain-
982 ing test inputs. We denoted the former set as “Unreliable” and denoted the latter
983 one as “Reliable”. We also compared the results such obtained with the original
984 accuracy reproduced by our approach, which is denoted as “Original”. Similar pro-
985 cedures were applied with respect to MR-2, and the MR-1&2. If the results before
986 and after removing the unreliable inference have a significant difference, it indi-
987 cates that the unreliable inferences will induce bias for model evaluation. We then
988 re-computed the accuracy based on each set of test inputs and checked if the eval-
989 uation results are significantly different by conducting the Wilcoxon signed-rank
990 test (Wilcoxon 1945).

991 6.3.3 Results and Discussion

992 Table 7 shows the results aggregated over all the 18 single-label image classification
993 models. In terms of the accuracy evaluated after removing the unreliable inferences
994 with respect to MR-2 (column *MR-2 Reliable*), it is significantly higher than the
995 original accuracy value obtained over all the test inputs ($p\text{-value} = 3.81 * e^{-6}$).
996 On average, the model accuracy after removing the unreliable inferences is 8.84%

Table 8: The Comparison of the Top-1 Accuracy between the Unreliable Inferences and Reliable Inferences for Multi-label Image Classification Models

Model	Original	MR-1		MR-2		MR-1&2	
		Unreliable	Reliable	Unreliable	Reliable	Unreliable	Reliable
ResNet50	34.5%	41.66%	34.17%	22.47%	48.29%	33.65%	34.49%
TResNet-L	45.5%	45.98%	45.51%	22.87%	72.45%	28.85%	46.19%
TResNet-XL	47.9%	45.31%	48.06%	23.19%	73.03%	25.84%	48.71%

997 (5.73%~12.31%) higher than the original accuracy. For MR-1 and MR-1&2, a
 998 certain trend toward significance could also be observed, for which the model
 999 accuracy after removing the unreliable inferences is only 1.31% (1.04%~1.55%)
 1000 and 1.30% (1.04%~1.52%) higher than the original accuracy.

1001 Table 8 shows the result of three multi-label classification models. Similar to the
 1002 previous finding for single-label classification models, after removing the unreliable
 1003 inferences violating MR-2, the model accuracy is much higher (13.79%~26.95%)
 1004 than the original accuracy value obtained over all the test inputs. Please note that
 1005 the significant test is not applicable since there are only three samples, which is
 1006 significantly less than 20, the typical minimum number for a significant test.

1007 The above results reveal that the existence of unreliable inferences violating
 1008 MR-2 causes significant bias for model evaluation, while the effect of unreliable
 1009 inferences violating MR-1 and MR-1&2 is limited. By excluding those unreliable
 1010 inferences violating MR-2, the performance of existing models evaluated with re-
 1011 spect to accuracy is much higher than that evaluated based on inputs containing
 1012 unreliable inferences. We suggest developers to remove unreliable inferences for
 1013 fair model comparisons, especially the inferences violating MR-2.

1014 Besides, in general, as shown in Table 7 and Table 8, the model accuracy
 1015 on the unreliable inference is significantly lower than the original accuracy of
 1016 model. However, there are some exceptions. In multi-label image classification
 1017 (Table 8), the model accuracy on the unreliable inference is higher than (ResNet50
 1018 and TResNet-L, MR-1) or close to (ResNet50, MR-1&2 and TResNet-XL, MR-1)
 1019 the original accuracy of the model. We suggest that the developers should pay more
 1020 attention to such exceptions: even if the unreliable inferences have a comparable
 1021 accuracy with the reliable ones, they may raise concerns on model reliability, as
 1022 we mentioned in Section 1.

1023 **Answer to RQ5** The unreliable inferences violating MR-2 can cause significant
 1024 effects (8.84% for single-label classification and 21.96% for multi-label classifica-
 1025 tion) on the evaluation results, thus inducing bias in model comparisons. On the
 1026 contrary, the effect of the unreliable inferences violating MR-1 and MR-1&2 is
 1027 limited.

1028 6.4 Taming Unreliable Inferences

1029 **RQ6** Can the unreliable inference be tamed during training?

1030 6.4.1 Motivation

1031 Previous results have shown that unreliable inferences generally exist in widely-
1032 used models built with different architectures. Besides, the inputs causing unreli-
1033 able inferences vary across models. These unreliable inferences can induce signif-
1034 icant bias in the evaluation of model performance. In this subsection, we studied
1035 whether such unreliable inferences can be tamed. Specifically, our study has two
1036 goals.

1037 First, we investigated whether the ratio of unreliable inferences can be re-
1038 duced during the model training process. Second, we investigated whether there
1039 is any correlation between model accuracy and the ratio of unreliable inferences.
1040 Understanding their correlation helps formulate a training strategy taming such
1041 unreliable inferences. For instance, if the top-1 accuracy is negatively correlated
1042 with the ratio of unreliable inference, the ratio of the unreliable inferences is likely
1043 to be reduced by enhancing the model accuracy.

1044 6.4.2 Experiment Setup

1045 We conducted two experiments with the aim to achieve the above two goals. First,
1046 we trained the VGG16 and Resnet50 models from scratch using the training source
1047 code provided by PyTorch official example repository,⁵ based on the ImageNet
1048 dataset. We selected these two models because they have been popularly adopted
1049 by existing studies for testing DNN systems (Pei et al. 2017; Ma et al. 2018a;
1050 Tian et al. 2020b; Zhao et al. 2017). The training was based on the default hyper-
1051 parameters, and stopped when its accuracy and loss reach saturation. We then
1052 measured the ratio of unreliable inferences in all correct inferences for every five
1053 epochs during the training process to see if they are reduced. Since the training
1054 process of DNN models is stochastic, we repeated the training three times for each
1055 model. Please note that the training of these two models is very time-consuming.
1056 Although our server has eight 2080Ti GPU cards, it still takes around 80 mins
1057 and 30 mins to train one epoch for VGG16 and Resnet50. The total training time
1058 spent for this experiment is more than 20 days.

1059 Second, we investigated the correlation between model accuracy and the ratio
1060 of unreliable inferences using the pre-trained models in Table 5. Specifically, we
1061 used the Pearson Correlation (Benesty et al. 2009) to check whether the ratio of
1062 unreliable inferences and the top-1 accuracy are correlated. We also plotted them
1063 for visualization.

1064 In this research question, we did not include the multi-label classification due
1065 to the following two reasons. First, the source code to train these models is not
1066 available. Second, the number of available multi-label classification models is lim-
1067 ited and it is not applicable to calculate the Pearson Correlation.

1068 6.4.3 Results and Discussion

1069 On average, our trained VGG16 and Resnet50 models achieve the top-1 accuracy
1070 of 72.1% and 76.1%, respectively. Their accuracy is close to the accuracy of the pre-

⁵ <https://github.com/pytorch/examples>

1071 trained models published by Pytorch,⁶ which are 71.6% and 76.2%, respectively.
1072 Figure 9 shows the top-1 accuracy and the ratio of unreliable inferences during
1073 the training stages. Please note the ratios of unreliable inferences violating MR-
1074 1&2 are not plotted as they are highly overlapped with the ratios of unreliable
1075 inferences violating MR-1.

1076 It can be observed that at the beginning of training, the ratio of unreliable infer-
1077 ences violating MR-2 decreases significantly and the ratio of unreliable inferences
1078 violating MR-1 slightly decreases. Later on, both of them become stable with the
1079 accuracy becoming saturated. Such results indicate that the current model train-
1080 ing methodologies can guide the models to learn object-relevant features to certain
1081 extents, as the ratio of unreliable inferences decreases at the first beginning. How-
1082 ever, they become less effective with the training epochs increases, as the ratio of
1083 unreliable inferences becomes stable after the beginning. In other words, they may
1084 not necessarily prevent the model from making unreliable inferences.

1085 We then investigated the correlation between the top-1 accuracy and the ratio
1086 of unreliable inferences based on the pre-trained models. The Pearson Correla-
1087 tion coefficients between the ratio of unreliable inferences violating MR-1, MR-2,
1088 and MR-1&2 with top-1 accuracy are 0.702, -0.901, and 0.492, respectively. Fig-
1089 ure 10 shows the relation of the ratio of unreliable inferences that violate MR and
1090 the top-1 accuracy, as well as their linear regression lines. The results indicate a
1091 strong negative correlation ($-0.901 < -0.9$) between the ratio of unreliable infer-
1092 ences violating MR-2 and top-1 accuracy. In other words, higher top-1 accuracy of
1093 a model couples with lower ratio of its unreliable inferences violating MR-2. The
1094 ratio of unreliable inferences violating MR-1 has a relatively positive correlation
1095 with top-1 accuracy. It increases very slightly with the increase in top-1 accuracy.
1096 The ratio of unreliable inferences violating MR-1&2 remains about the same. This
1097 may be because that the ratio of unreliable inference violating MR-1 and MR-1&2
1098 is relatively small and their changes are not obvious.

1099 **Answer to RQ6** The current training methodologies can help the models to
1100 reduce the unreliable inference to certain extents, but they become less effective
1101 with the training epochs increases and may not necessarily prevent the model from
1102 making unreliable inferences.

1103 7 Limitation and Future Work

1104 Our study points out that unreliable inferences commonly exist in the DNN-based
1105 image classification models. In this section, we discuss some limitations of our
1106 work and the future work. In the future, we will explore the possibility to improve
1107 the reliability of inferences made by DNN models and address such unreliable
1108 inferences effectively and efficiently.

1109 7.1 Other Possible MRs

1110 We introduced our approach for the MR-1 and MR-2 in Section 4. There are al-
1111 ternative approaches. For example, in the multi-label classification, we consider

⁶ <https://pytorch.org/docs/stable/torchvision/models.html>

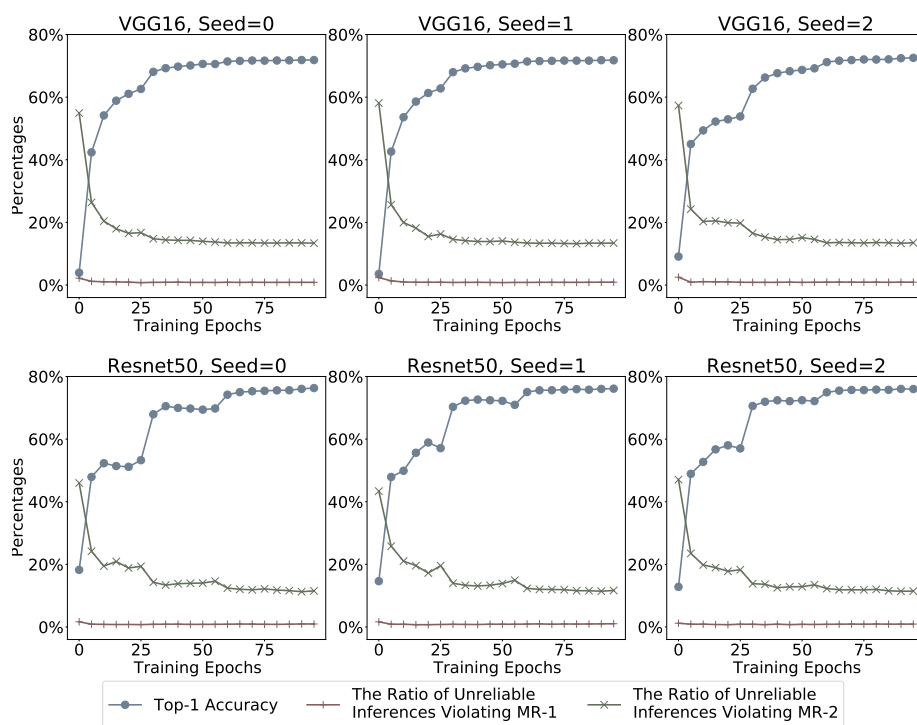


Fig. 9: The Top-1 Accuracy and the Ratio of Unreliable Inferences of VGG16/Resnet50 during Training

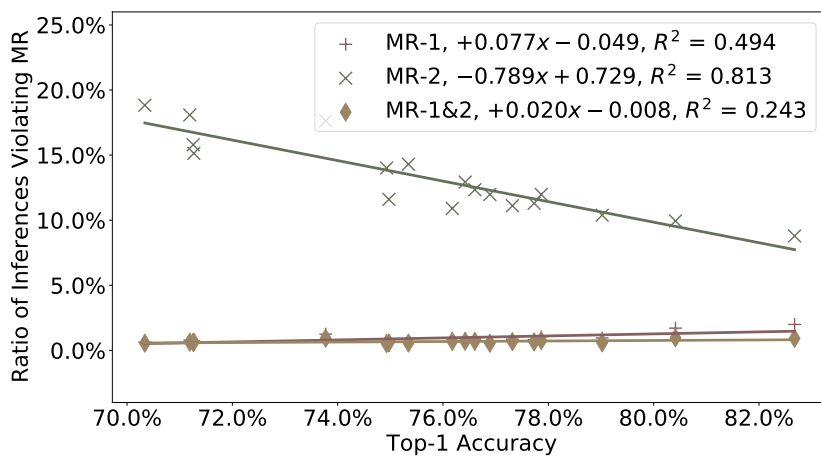


Fig. 10: The Relationship between Top-1 Accuracy and the Ratio of Unreliable Inferences Violating MRs for Single-Label Image Classification Models on the ImageNet Dataset

1112 the union of all the objects holistically and mutate them all together. An alter-
 1113 native way is to consider each label one by one. For example, we only mutate all
 1114 objects belonging to a specific label at one time and then examine whether this
 1115 label violates the MR. After examining all labels, one can conclude whether the
 1116 inference violates the MR. Such an alternative will increase the workload and re-
 1117 quires a more sophisticated methodology to judge whether an inference is reliable
 1118 based on all its labels. We believe there are several potential ways to define such
 1119 methodology, thus we leave it as future work to conduct an exhausting study.

1120 Further, for multi-label classification, exact match (Wu and Zhu 2020) is used
 1121 in the comparison of the certainty, i.e., $\mathcal{C}(L_{\mathcal{M}(i)}) > \mathcal{C}(L_{\mathcal{M}(i'_c)}) \iff \mathcal{C}_{l,\mathcal{M}(i)} >$
 1122 $\mathcal{C}_{l,\mathcal{M}(i'_c)}, \forall l \in L_{\mathcal{M}(i)}$. The comparison can use other metrics, such as Hamming
 1123 Loss and Jaccard Index. In the future, one may investigate the effect of different
 1124 metrics in the comparison.

1125 7.2 Other Potential Application Scenarios

1126 In our study, we focus on the applications of the DNN on image classification.
 1127 After proper adaption, our MRs can be applied to other applications used on DNN,
 1128 such as object detection (Liu et al. 2016; Ren et al. 2017; Redmon et al. 2016) and
 1129 language processing (Devlin et al. 2019). For example, in object detection, one
 1130 may examine the object-relevancy for each detected object. The corresponding
 1131 MRs can be:⁷

1132 **MR-3:** An image mutated by corrupting only the features of the target ob-
 1133 ject(s) should lead to an inference result with different label(s) and location(s), or
 1134 an inference result with the same label(s) and location(s) but with less certainty.

1135 **MR-4:** An image mutated by preserving the features of the target object(s)
 1136 and corrupting other features should lead to an inference result with the same
 1137 label(s) and location(s).

1138 As for language processing, the MR could be:

1139 **MR-5:** A sentence mutated by corrupting only the content words should lead
 1140 to a different inference result.

1141 **MR-6:** A sentence mutated by preserving the content words and corrupting
 1142 other function words should lead to a similar inference result.

1143 Future work can target proposing new MRs for other DNN-based applications
 1144 and study their effectiveness.

1145 7.3 False Positives and False Negatives

1146 The mutations used in our approach can unnecessarily import/remove extra fea-
 1147 tures and then bring some side effects, such as false positives/negatives. Although
 1148 we applied three mutation operators and adopted the majority voting to alleviate
 1149 this threat, it still may happen. In the future work, we will explore different image
 1150 mutation methods and reduce such possible side effects, including false negatives
 1151 and false positives.

⁷ The MR-3/4/5/6 are just our initial proposals. The detailed definition should be polished and their effectiveness should be thoroughly evaluated.

1152 In our evaluation, we only evaluate the effectiveness of our approach from
1153 the perspective of true positives and false positives, but not the false negatives,
1154 which are the inferences that are based on the object-irrelevant features but are
1155 not detected by our approach. It is challenging to identify the false negatives,
1156 since it is hard to know whether the inference is indeed completely based on the
1157 object-irrelevant features, which is an outstanding challenge in deep learning (see
1158 Section 8.3 and 8.4), and whether the changes of the certainty is caused by the
1159 imported/removed features in the mutation. We believe it will be one of the future
1160 work directions.

1161 7.4 The Effect of Annotation Formats

1162 Our metamorphic approach leverages the annotation of the object to construct the
1163 follow-up inputs. The availability and the quality of the annotation could affect the
1164 performance of our approach. This is the major limitation of our study. As shown
1165 in the evaluation in Section 5, inappropriate annotations are the major sources of
1166 false positives. In the future work, we will explore new methodologies to alleviate
1167 this limitation.

1168 In our study, we use bounding boxes for single-label classification and object
1169 masks for multi-label classification, depending on their availability in the datasets.
1170 We would like to point out that the annotation format could also affect the effec-
1171 tiveness of our approach. For example, if the annotation is in the format of object
1172 mask, even after the object corruption in MR-1, the object shape could still be
1173 left in the follow-up inputs, which may cause false positives for MR-1 (similar to
1174 the incomplete removal of the target object). According to a recent study (Geirhos
1175 et al. 2019), the texture of the input image, rather than its shape, has stronger
1176 impact in DNN-based image classifications. In other words, “*a cat with an elephant
1177 texture is an elephant to CNNs, and still a cat to humans*” (Geirhos et al. 2019).
1178 Thus, the influence of the shape information left in the follow-up inputs should be
1179 limited. Nevertheless, we would like to point out this possible factor and interested
1180 researchers may explore along this direction in the future. A possible countermea-
1181 sure is to develop a novel mutation methodology such that it will further remove
1182 the shape information. For example, we can add random padding to the object
1183 boundary, so that the image shape information will be destroyed.

1184 8 Related Work

1185 8.1 Metamorphic Testing in DNN models

1186 Several studies have applied metamorphic testing to validate DNN models (Xie
1187 et al. 2011; Ding et al. 2017; Dwarakanath et al. 2018; Zhang et al. 2018; Tian
1188 et al. 2018). Dwarakanath et al. (Dwarakanath et al. 2018) leveraged two sets of
1189 metamorphic relations to identify faults in machine learning implementations. For
1190 example, one metamorphic relation is that the “permutation of input channels (i.e.
1191 RGB channels) for the training and test data” would not affect inference results.
1192 To validate whether a specific implementation of DNN satisfies this relation, they
1193 re-ordered the RGB channel of images in both the training set and test set. They

1194 examine the impact on the accuracy or precision of the DNN model after it is
1195 trained using the permuted dataset. Their relations treat the pixels in an image as
1196 independent units and they do not consider objects and background in the image.

1197 Xie et al. (Xie et al. 2011) performed metamorphic testing on two machine
1198 learning algorithms: k-Nearest Neighbors and Naïve Bayes Classifier. Their work
1199 targets testing attribute-based machine learning models instead of deep learning
1200 systems. Ding et al. (Ding et al. 2017) proposed metamorphic relations for DNN at
1201 three different validation levels: system level, data set level and data item level. For
1202 example, a metamorphic relation on system level asserts that DNNs should per-
1203 form better than SVM classifiers for image classification. Their technique requires
1204 retraining the systems and is inapplicable to testing pre-trained models.

1205 Other studies (Zhang et al. 2018; Tian et al. 2018; Zhou and Sun 2019) lever-
1206 aged metamorphic testing to validate autonomous driving systems. DeepTest (Tian
1207 et al. 2018) designed a systematic testing approach to detecting the inconsistent
1208 behaviors of autonomous driving systems using metamorphic relation. Their rela-
1209 tions focus on general image transformation, including scale, shear, rotation and
1210 so on. Further, DeepRoad (Zhang et al. 2018) leverages Generative Adversarial
1211 Networks to improve the quality of the transformed images. Given an autonomous
1212 driving system, DeepRoad mutates the original images to simulate weather condi-
1213 tions such as adding fog to an image. An inconsistency is identified if a DNN
1214 model and its mutant make an inconsistent decision on an image (e.g., the dif-
1215 ference of the steering degrees exceeds a certain threshold). Differently from the
1216 existing study, we design metamorphic relations to assess whether an inference is
1217 based on object-relevant features for DNN-based image classification models.

1218 8.2 Testing Deep Learning Systems

1219 Besides metamorphic testing, studies have also been made to adapt other classical
1220 testing techniques for DNN models. A recent survey (Zhang et al. 2020) sum-
1221 marizes the latest work in this direction. DeepXplore (Pei et al. 2017) proposed
1222 neuron coverage to quantify the adequacy of a testing dataset. DeepGauge (Ma
1223 et al. 2018a) proposed a collection of testing criteria. TensorFuzz (Odena et al.
1224 2019), DLFuzz (Guo et al. 2018) and DeepHunter (Xie et al. 2019a) leveraged
1225 fuzz testing to facilitate the debugging process in DNN. DeepMutation (Ma et al.
1226 2018b) applied mutation testing to measure the quality of test data in DNN. Our
1227 study falls into the research direction of testing DNN systems. One of our major
1228 contributions is that we test DNN models from a new perspective, i.e., the object
1229 relevancy of inferences.

1230 8.3 Background Dependence of Computer Vision Systems

1231 Some existing work studied the background dependence of computer vision sys-
1232 tems, even before the DNN becomes popular (Roobaert et al. 2001; Qin et al.
1233 2010). Qin et al. (Qin et al. 2010) found that removing the background in street
1234 scene images can improve the performance of object recognition systems. Rosen-
1235 feld et al. (Rosenfeld et al. 2018) demonstrated that after transplanting an object

1236 from the training set to the background of another image, the state-of-the-art ob-
1237 ject detectors could fail to identify the inserted object. Later, Wang and Su (Wang
1238 and Su 2020) proposed an automated approach to test the object detectors. Their
1239 approach generates test inputs by inserting objects to another image’s background.
1240 Our study focuses on image classification applications, and we conduct a large-
1241 scale empirical study to understand the problem.

1242 8.4 Heatmap-based Testing of DNN Models

1243 Researchers have proposed ideas of generating *HeatMaps* for DNN testing and de-
1244 bugging (Ribeiro et al. 2016; Zhou et al. 2016; Selvaraju et al. 2017; Ma et al.
1245 2018c; Montavon et al. 2019; Fahmy et al. 2020). These HeatMaps essentially cap-
1246 ture the *importance* of individual neurons (Ma et al. 2018c) or layers (Montavon
1247 et al. 2019; Fahmy et al. 2020) in a given DNN model. Based on different defi-
1248 nitions of *importance*, these methods generate different types of HeatMaps. Some
1249 of them directly use neuron activation values, gradient values etc. for HeatMap
1250 generation (Zhou et al. 2016; Selvaraju et al. 2017). Others perform some extra
1251 processing on such raw data, such as calculating the Jacobian matrix or using
1252 differential analysis to extract the differences between correctly classified and mis-
1253 classified samples (Ma et al. 2018c). A common drawback of such methods is that
1254 there is no standard definition of neuron/layer importance and it is hard to eval-
1255 uate whether the generated HeatMaps are correct. As a result, these HeatMaps
1256 may or may not accurately reflect neuron/layer importance. Compared to their
1257 work, the effectiveness of our approach is properly evaluated.

1258 Moreover, some HeatMap generation techniques require the intermediate infor-
1259 mation from the models and can only be applied for some specific types of models.
1260 For example, CAM (Zhou et al. 2016) and GradCAM (Zhou et al. 2016) requires
1261 access to the pooling layer of neural networks, which may not always be available.
1262 Different from these methods, our method does not need extra intermediate re-
1263 sults from models and thus can be applied to any DNN-based image classification
1264 models.

1265 9 Acknowledgment

1266 We want to thank all reviewers for their constructive comments and suggestions for
1267 the manuscript. We would also like to thank the editors’ coordination. We would
1268 like to express our deep gratitude to Miss Yao Feng for her significant contribution
1269 to the manual check. Besides, we appreciate the proofreading by our labmates, Mr.
1270 Wuqi Zhang, Mr. Meiziniu Li, Mr. Hao Guan and Miss Lei Liu.

1271 This work was supported by the National Key Research and Development Pro-
1272 gram of China (Grant No. 2019YFE0198100), National Natural Science Founda-
1273 tion of China (Grant No. 61932021, 62002125 and 61802164), Guangdong Provin-
1274 cial Key Laboratory (Grant No. 2020B121201001), Hong Kong RGC/RIF (Grant
1275 No. R5034-18), Hong Kong ITF (Grant No: MHP/055/19), Hong Kong PhD Fel-
1276 lowship Scheme, MSRA Collaborative Research Grant, Microsoft Cloud Research
1277 Software Fellow Award 2019, NSF 1901242, NSF 1910300, and IARPA TrojAI

1278 W911NF19S0012. Any opinions, findings, and conclusions in this paper are those
1279 of the authors only and do not necessarily reflect the views of our sponsors.

1280 10 Conclusion

1281 In this work, we proposed to leverage metamorphic testing to identify unreliable
1282 image classifications made by DNN models based on object-irrelevant features.
1283 We proposed two metamorphic relations, from the perspective of object relevancy.
1284 We evaluated the effectiveness of our approach and showed that it achieves high
1285 precision. We applied our approach to 21 popular pre-trained DNN models with
1286 the ImageNet and COCO datasets, and found that the phenomenon of unreliable
1287 inferences is pervasive. The pervasiveness caused significant bias in model eval-
1288 uation. Our experiments revealed that the current model training methodologies
1289 can guide the models to learn object-relevant features to certain extent, but may
1290 not necessarily prevent the model from making unreliable inferences. Therefore,
1291 further research is needed to develop a more effective approach for enhancing a
1292 model’s object-relevancy property.

1293 References

- 1294 Aggarwal A, Lohia P, Nagar S, Dey K, Saha D (2019) Black box fairness testing of machine
1295 learning models. In: Proceedings of the 2019 27th ACM Joint Meeting on European Soft-
1296 ware Engineering Conference and Symposium on the Foundations of Software Engineering,
1297 Association for Computing Machinery, New York, NY, USA, ESEC/FSE 2019, p 625–635,
1298 DOI 10.1145/3338906.3338937, URL <https://doi.org/10.1145/3338906.3338937>
- 1299 Barr ET, Harman M, McMinn P, Shahbaz M, Yoo S (2015) The oracle problem in software
1300 testing: A survey. *IEEE Transactions on Software Engineering* 41(5):507–525
- 1301 Ben-Baruch E, Ridnik T, Zamir N, Noy A, Friedman I, Protter M, Zelnik-Manor L (2020)
1302 Asymmetric loss for multi-label classification. 2009.14119
- 1303 Benesty J, Chen J, Huang Y, Cohen I (2009) Pearson correlation coefficient. In: Noise reduction
1304 in speech processing, Springer, pp 1–4
- 1305 Carlini N, Wagner DA (2017) Towards evaluating the robustness of neural networks. In: 2017
1306 IEEE Symposium on Security and Privacy, SP 2017, San Jose, CA, USA, May 22–26, 2017,
1307 IEEE Computer Society, pp 39–57, DOI 10.1109/SP.2017.49, URL <https://doi.org/10.1109/SP.2017.49>
- 1308
- 1309 Chen TY, Cheung SC, Yiu SM (1998) Metamorphic testing: a new approach for generating
1310 next test cases. Tech. Rep. HKUST-CS98-01, Department of Computer Science, Hong
1311 Kong University of Science and Technology, Hong Kong
- 1312 Chen TY, Kuo FC, Liu H, Poon PL, Towey D, Tse TH, Zhou ZQ (2018) Metamorphic testing:
1313 A review of challenges and opportunities. *ACM Comput Surv* 51(1):4:1–4:27, DOI 10.
1314 1145/3143561, URL <http://doi.acm.org/10.1145/3143561>
- 1315 Chollet F, et al. (2015a) Keras. <https://keras.io>
- 1316 Chollet F, et al. (2015b) Keras applications. URL <https://keras.io/api/applications/>
- 1317 Cochran W (1963) Sampling techniques. 2nd edition. [Wiley Publications in Statistics.], John
1318 Wiley & Sons
- 1319 Cramer H (1946) Mathematical methods of statistics. Princeton University Press, Princeton
- 1320 Deng J, Dong W, Socher R, Li LJ, Li K, Fei-Fei L (2009) ImageNet: A Large-Scale Hierarchical
1321 Image Database. In: CVPR09
- 1322 Devlin J, Chang M, Lee K, Toutanova K (2019) BERT: pre-training of deep bidirectional
1323 transformers for language understanding. In: Burstein J, Doran C, Solorio T (eds)
1324 Proceedings of the 2019 Conference of the North American Chapter of the Associa-
1325 tion for Computational Linguistics: Human Language Technologies, NAACL-HLT 2019,

- 1326 Minneapolis, MN, USA, June 2-7, 2019, Volume 1 (Long and Short Papers), Association
1327 for Computational Linguistics, pp 4171–4186, DOI 10.18653/v1/n19-1423, URL
1328 <https://doi.org/10.18653/v1/n19-1423>
- 1329 Ding J, Kang X, Hu X (2017) Validating a deep learning framework by metamorphic testing.
1330 In: 2017 IEEE/ACM 2nd International Workshop on Metamorphic Testing (MET), pp
1331 28–34, DOI 10.1109/MET.2017.2
- 1332 Dwarakanath A, Ahuja M, Sikand S, Rao RM, Bose RPJC, Dubash N, Podder S (2018)
1333 Identifying implementation bugs in machine learning based image classifiers using meta-
1334 morphic testing. In: Proceedings of the 27th ACM SIGSOFT International Symposium
1335 on Software Testing and Analysis, ACM, New York, NY, USA, ISSTA 2018, pp 118–128,
1336 DOI 10.1145/3213846.3213858, URL <http://doi.acm.org/10.1145/3213846.3213858>
- 1337 Fahmy H, Pastore F, Bagherzadeh M, Briand L (2020) Supporting dnn safety analysis and
1338 retraining through heatmap-based unsupervised learning. 2002.00863
- 1339 Fellbaum C (2006) Wordnet(s). In: Brown K (ed) Encyclopedia of Language & Linguistics (Sec-
1340 ond Edition), second edition edn, Elsevier, Oxford, pp 665 – 670, DOI <https://doi.org/10.1016/B0-08-044854-2/00946-9>, URL <http://www.sciencedirect.com/science/article/pii/B0080448542009469>
- 1341 Freund Y, Schapire RE (1995) A decision-theoretic generalization of on-line learning and an ap-
1342 plication to boosting. In: Vitányi P (ed) Computational Learning Theory, Springer Berlin
1343 Heidelberg, Berlin, Heidelberg, pp 23–37
- 1344 FRS KP (1900) X. on the criterion that a given system of deviations from the probable in
1345 the case of a correlated system of variables is such that it can be reasonably supposed
1346 to have arisen from random sampling. The London, Edinburgh, and Dublin Philosophical
1347 Magazine and Journal of Science 50(302):157–175, DOI 10.1080/14786440009463897, URL
1348 <https://doi.org/10.1080/14786440009463897>
- 1349 Geirhos R, Rubisch P, Michaelis C, Bethge M, Wichmann FA, Brendel W (2019) Imagenet-
1350 trained cnns are biased towards texture; increasing shape bias improves accuracy and
1351 robustness. In: 7th International Conference on Learning Representations, ICLR 2019,
1352 New Orleans, LA, USA, May 6-9, 2019, OpenReview.net, URL <https://openreview.net/forum?id=Bygh9j09KX>
- 1353 Gu T, Liu K, Dolan-Gavitt B, Garg S (2019) Badnets: Evaluating backdoor attacks on deep
1354 neural networks. IEEE Access 7:47230–47244, DOI 10.1109/ACCESS.2019.2909068
- 1355 Guo J, Jiang Y, Zhao Y, Chen Q, Sun J (2018) Dlfuzz: Differential fuzzing testing of deep
1356 learning systems. In: Proceedings of the 2018 26th ACM Joint Meeting on European Soft-
1357 ware Engineering Conference and Symposium on the Foundations of Software Engineering,
1358 Association for Computing Machinery, New York, NY, USA, ESEC/FSE 2018, p 739–743,
1359 DOI 10.1145/3236024.3264835, URL <https://doi.org/10.1145/3236024.3264835>
- 1360 He K, Zhang X, Ren S, Sun J (2016) Deep residual learning for image recognition. In: 2016
1361 IEEE Conference on Computer Vision and Pattern Recognition (CVPR), pp 770–778,
1362 DOI 10.1109/CVPR.2016.90
- 1363 Howard AG, Zhu M, Chen B, Kalenichenko D, Wang W, Weyand T, Andreetto M, Adam H
1364 (2017) Mobilenets: Efficient convolutional neural networks for mobile vision applications.
1365 CoRR abs/1704.04861, URL <http://arxiv.org/abs/1704.04861>, 1704.04861
- 1366 Huang G, Liu Z, van der Maaten L, Weinberger KQ (2017) Densely connected convolutional
1367 networks. In: 2017 IEEE Conference on Computer Vision and Pattern Recognition, CVPR
1368 2017, Honolulu, HI, USA, July 21-26, 2017, IEEE Computer Society, pp 2261–2269, DOI
1369 10.1109/CVPR.2017.243, URL <https://doi.org/10.1109/CVPR.2017.243>
- 1370 Krasin I, Duerig T, Alldrin N, Ferrari V, Abu-El-Haija S, Kuznetsova A, Rom H, Uijlings J,
1371 Popov S, Kamali S, Mallocci M, Pont-Tuset J, Veit A, Belongie S, Gomes V, Gupta A,
1372 Sun C, Chechik G, Cai D, Feng Z, Narayanan D, Murphy K (2017) Openimages: A public
1373 dataset for large-scale multi-label and multi-class image classification. Dataset available
1374 from <https://storage.googleapis.com/openimages/web/index.html>
- 1375 Krizhevsky A, Nair V, Hinton G (2009) The cifar-10 dataset. URL <http://www.cs.toronto.edu/~kriz/cifar.html>
- 1376 Krizhevsky A, Sutskever I, Hinton GE (2012) Imagenet classification with deep
1377 convolutional neural networks. In: Pereira F, Burges CJC, Bottou L, Wein-
1378 berger KQ (eds) Advances in Neural Information Processing Systems 25,
1379 Curran Associates, Inc., pp 1097–1105, URL <http://papers.nips.cc/paper/4824-imagenet-classification-with-deep-convolutional-neural-networks.pdf>

- 1385 Landis JR, Koch GG (1977) The measurement of observer agreement for categorical data.
1386 *Biometrics* 33(1):159–174
- 1387 LeCun Y, Cortes C (2010) MNIST handwritten digit database.
1388 <http://yann.lecun.com/exdb/mnist/>, URL <http://yann.lecun.com/exdb/mnist/>
- 1389 Lin T, Maire M, Belongie SJ, Bourdev LD, Girshick RB, Hays J, Perona P, Ramanan D, Dollár
1390 P, Zitnick CL (2014) Microsoft COCO: common objects in context. CoRR abs/1405.0312,
1391 URL <http://arxiv.org/abs/1405.0312>, 1405.0312
- 1392 Lin Y, Lv F, Zhu S, Yang M, Cour T, Yu K, Cao L, Huang T (2011) Large-scale image
1393 classification: Fast feature extraction and svm training. In: CVPR 2011, pp 1689–1696
- 1394 Liu W, Anguelov D, Erhan D, Szegedy C, Reed S, Fu CY, Berg AC (2016) Ssd: Single shot
1395 multibox detector. In: Leibe B, Matas J, Sebe N, Welling M (eds) *Computer Vision –*
1396 *ECCV 2016*, Springer International Publishing, Cham, pp 21–37
- 1397 Ma L, Juefei-Xu F, Zhang F, Sun J, Xue M, Li B, Chen C, Su T, Li L, Liu Y, Zhao J,
1398 Wang Y (2018a) Deepgauge: Multi-granularity testing criteria for deep learning systems.
1399 In: *Proceedings of the 33rd ACM/IEEE International Conference on Automated Software*
1400 *Engineering*, ACM, New York, NY, USA, ASE 2018, pp 120–131, DOI 10.1145/3238147.
1401 3238202, URL <http://doi.acm.org/10.1145/3238147.3238202>
- 1402 Ma L, Zhang F, Sun J, Xue M, Li B, Juefei-Xu F, Xie C, Li L, Liu Y, Zhao J, Wang Y (2018b)
1403 Deepmutation: Mutation testing of deep learning systems. In: Ghosh S, Natella R, Cukic B,
1404 Poston R, Laranjeiro N (eds) *29th IEEE International Symposium on Software Reliability*
1405 *Engineering*, ISSRE 2018, Memphis, TN, USA, October 15-18, 2018, IEEE Computer
1406 Society, pp 100–111, DOI 10.1109/ISSRE.2018.00021, URL <https://doi.org/10.1109/ISSRE.2018.00021>
- 1408 Ma S, Liu Y, Lee WC, Zhang X, Grama A (2018c) Mode: Automated neural network model
1409 debugging via state differential analysis and input selection. In: *Proceedings of the 2018*
1410 *26th ACM Joint Meeting on European Software Engineering Conference and Symposium*
1411 *on the Foundations of Software Engineering*, Association for Computing Machinery, New
1412 York, NY, USA, ESEC/FSE 2018, p 175–186, DOI 10.1145/3236024.3236082, URL <https://doi.org/10.1145/3236024.3236082>
- 1414 Montavon G, Binder A, Lapuschkin S, Samek W, Müller KR (2019) Layer-wise relevance
1415 propagation: an overview. In: *Explainable AI: interpreting, explaining and visualizing deep*
1416 *learning*, Springer, pp 193–209
- 1417 Moosavi-Dezfooli S, Fawzi A, Frossard P (2016) Deepfool: A simple and accurate method to
1418 fool deep neural networks. In: *2016 IEEE Conference on Computer Vision and Pattern*
1419 *Recognition (CVPR)*, pp 2574–2582, DOI 10.1109/CVPR.2016.282
- 1420 Nejadgholi M, Yang J (2019) A study of oracle approximations in testing deep learning libraries.
1421 In: *2019 34th IEEE/ACM International Conference on Automated Software Engineering*
1422 *(ASE)*, pp 785–796, DOI 10.1109/ASE.2019.00078
- 1423 Odena A, Olsson C, Andersen D, Goodfellow IJ (2019) Tensorfuzz: Debugging neural networks
1424 with coverage-guided fuzzing. In: Chaudhuri K, Salakhutdinov R (eds) *Proceedings of the*
1425 *36th International Conference on Machine Learning*, ICML 2019, 9-15 June 2019, Long
1426 Beach, California, USA, PMLR, *Proceedings of Machine Learning Research*, vol 97, pp
1427 4901–4911, URL <http://proceedings.mlr.press/v97/odena19a.html>
- 1428 Pei K, Cao Y, Yang J, Jana S (2017) Deepxplore: Automated whitebox testing of deep learning
1429 systems. In: *Proceedings of the 26th Symposium on Operating Systems Principles*, ACM,
1430 New York, NY, USA, SOSP '17, pp 1–18, DOI 10.1145/3132747.3132785, URL <http://doi.acm.org/10.1145/3132747.3132785>
- 1432 Pham HV, Lutellier T, Qi W, Tan L (2019) CRADLE: cross-backend validation to detect and
1433 localize bugs in deep learning libraries. In: *Proceedings of the 41st International Conference*
1434 *on Software Engineering*, IEEE Press, ICSE '19, p 1027–1038, DOI 10.1109/ICSE.2019.
1435 00107, URL <https://doi.org/10.1109/ICSE.2019.00107>
- 1436 Qin G, Vrusias B, Gillam L (2010) Background filtering for improving of object detection
1437 in images. In: *2010 20th International Conference on Pattern Recognition*, pp 922–925,
1438 DOI 10.1109/ICPR.2010.231
- 1439 Redmon J, Divvala S, Girshick R, Farhadi A (2016) You only look once: Unified, real-time
1440 object detection. In: *2016 IEEE Conference on Computer Vision and Pattern Recognition*
1441 *(CVPR)*, pp 779–788, DOI 10.1109/CVPR.2016.91
- 1442 Ren S, He K, Girshick R, Sun J (2017) Faster r-cnn: Towards real-time object detection with
1443 region proposal networks. *IEEE Transactions on Pattern Analysis and Machine Intelligence*
1444 39(6):1137–1149, DOI 10.1109/TPAMI.2016.2577031

- 1445 Ribeiro MT, Singh S, Guestrin C (2016) "why should I trust you?": Explaining the predictions
1446 of any classifier. In: Proceedings of the 22nd ACM SIGKDD International Conference on
1447 Knowledge Discovery and Data Mining, San Francisco, CA, USA, August 13-17, 2016, pp
1448 1135–1144
- 1449 Roobaert D, Zillich M, Eklundh J (2001) A pure learning approach to background-invariant
1450 object recognition using pedagogical support vector learning. In: Proceedings of the 2001
1451 IEEE Computer Society Conference on Computer Vision and Pattern Recognition. CVPR
1452 2001, vol 2, pp II–II, DOI 10.1109/CVPR.2001.990982
- 1453 Rosenfeld A, Zemel RS, Tsotsos JK (2018) The elephant in the room. CoRR abs/1808.03305,
1454 URL <http://arxiv.org/abs/1808.03305>, 1808.03305
- 1455 Sanchez J, Perronnin F (2011) High-dimensional signature compression for large-scale image
1456 classification. In: Proceedings of the 2011 IEEE Conference on Computer Vision
1457 and Pattern Recognition, IEEE Computer Society, USA, CVPR '11, p 1665–1672, DOI
1458 10.1109/CVPR.2011.5995504, URL <https://doi.org/10.1109/CVPR.2011.5995504>
- 1459 Selvaraju RR, Cogswell M, Das A, Vedantam R, Parikh D, Batra D (2017) Grad-cam: Visual
1460 explanations from deep networks via gradient-based localization. In: IEEE International
1461 Conference on Computer Vision, ICCV 2017, Venice, Italy, October 22-29, 2017, IEEE
1462 Computer Society, pp 618–626, DOI 10.1109/ICCV.2017.74, URL <https://doi.org/10.1109/ICCV.2017.74>
- 1463 Simonyan K, Zisserman A (2015) Very deep convolutional networks for large-scale image recog-
1464 nition. In: Bengio Y, LeCun Y (eds) 3rd International Conference on Learning Representations,
1465 ICLR 2015, San Diego, CA, USA, May 7-9, 2015, Conference Track Proceedings
- 1466 Stock P, Cissac M (2018) Convnets and imagenet beyond accuracy: Understanding mistakes
1467 and uncovering biases. In: Ferrari V, Hebert M, Sminchisescu C, Weiss Y (eds) Com-
1468 puter Vision - ECCV 2018 - 15th European Conference, Munich, Germany, September
1469 8-14, 2018, Proceedings, Part VI, Springer, Lecture Notes in Computer Science, vol
1470 11210, pp 504–519, DOI 10.1007/978-3-030-01231-1_31, URL https://doi.org/10.1007/978-3-030-01231-1_31
- 1471 Tian Y, Pei K, Jana S, Ray B (2018) Deeptest: Automated testing of deep-neural-network-
1472 driven autonomous cars. In: Proceedings of the 40th International Conference on Software
1473 Engineering, ACM, New York, NY, USA, ICSE '18, pp 303–314, DOI 10.1145/3180155.
1474 3180220, URL <http://doi.acm.org/10.1145/3180155.3180220>
- 1475 Tian Y, Zeng Z, Wen M, Liu Y, Kuo Ty, Cheung SC (2020a) Evaldnn: A toolbox for evalu-
1476 ating deep neural network models. In: Proceedings of the ACM/IEEE 42nd International
1477 Conference on Software Engineering: Companion Proceedings, Association for Computing
1478 Machinery, New York, NY, USA, ICSE '20, p 45–48, DOI 10.1145/3377812.3382133, URL
1479 <https://doi.org/10.1145/3377812.3382133>
- 1480 Tian Y, Zhong Z, Ordonez V, Kaiser G, Ray B (2020b) Testing dnn image classifiers for
1481 confusion & bias errors. In: Proceedings of the ACM/IEEE 42nd International Conference
1482 on Software Engineering, Association for Computing Machinery, New York, NY, USA,
1483 ICSE '20, p 1122–1134, DOI 10.1145/3377811.3380400, URL <https://doi.org/10.1145/3377811.3380400>
- 1484 Tramèr F, Atlidakis V, Geambasu R, Hsu D, Hubaux J, Humbert M, Juels A, Lin H (2017)
1485 Fairtest: Discovering unwarranted associations in data-driven applications. In: 2017 IEEE
1486 European Symposium on Security and Privacy (EuroS P), pp 401–416, DOI 10.1109/
1487 EuroSP.2017.29
- 1488 Wang S, Su Z (2020) Metamorphic object insertion for testing object detection systems. In:
1489 Proceedings of the 35th ACM/IEEE International Conference on Automated Software
1490 Engineering, ACM, New York, NY, USA, ASE 2020, pp 1053–1065, DOI 10.1145/3324884.
1491 3416584, URL <http://doi.acm.org/10.1145/3324884.3416584>
- 1492 Wilcoxon F (1945) Individual comparisons by ranking methods. *Biometrics Bulletin* 1(6):80–83
- 1493 Wu G, Zhu J (2020) Multi-label classification: do hamming loss and subset accu-
1494 racy really conflict with each other? In: Larochelle H, Ranzato M, Hadsell R, Bal-
1495 can M, Lin H (eds) Advances in Neural Information Processing Systems 33: An-
1496 nual Conference on Neural Information Processing Systems 2020, NeurIPS 2020, De-
1497 cember 6-12, 2020, virtual, URL <https://proceedings.neurips.cc/paper/2020/hash/20479c788fb27378c2c99eadcf207e7f-Abstract.html>
- 1498 Xie X, Ho JW, Murphy C, Kaiser G, Xu B, Chen TY (2011) Testing and validating machine
1499 learning classifiers by metamorphic testing. *Journal of Systems and Software* 84(4):544
1500 – 558, DOI <https://doi.org/10.1016/j.jss.2010.11.920>, URL <http://www.sciencedirect.com>

- 1505 [com/science/article/pii/S0164121210003213](https://doi.org/10.1145/3293882.3330579), the Ninth International Conference on
1506 Quality Software
- 1507 Xie X, Ma L, Juefei-Xu F, Xue M, Chen H, Liu Y, Zhao J, Li B, Yin J, See S (2019a) Deep-
1508 hunter: a coverage-guided fuzz testing framework for deep neural networks. In: Zhang D,
1509 Møller A (eds) Proceedings of the 28th ACM SIGSOFT International Symposium on Soft-
1510 ware Testing and Analysis, ISSTA 2019, Beijing, China, July 15-19, 2019, ACM, pp 146-
1511 157, DOI 10.1145/3293882.3330579, URL <https://doi.org/10.1145/3293882.3330579>
- 1512 Xie X, Ma L, Wang H, Li Y, Liu Y, Li X (2019b) Diffchaser: Detecting disagreements for
1513 deep neural networks. In: Proceedings of the Twenty-Eighth International Joint Con-
1514 ference on Artificial Intelligence, IJCAI-19, International Joint Conferences on Artifi-
1515 cial Intelligence Organization, pp 5772-5778, DOI 10.24963/ijcai.2019/800, URL <https://doi.org/10.24963/ijcai.2019/800>
- 1516 Yu J, Lin Z, Yang J, Shen X, Lu X, Huang TS (2018) Generative image inpainting with contex-
1517 tual attention. In: 2018 IEEE Conference on Computer Vision and Pattern Recognition,
1518 CVPR 2018, Salt Lake City, UT, USA, June 18-22, 2018, IEEE Computer Society, pp
1519 5505-5514, DOI 10.1109/CVPR.2018.00577
- 1520 Zhang JM, Harman M, Ma L, Liu Y (2020) Machine learning testing: Survey, landscapes and
1521 horizons. IEEE Transactions on Software Engineering pp 1-1, DOI 10.1109/TSE.2019.
1522 2962027
- 1523 Zhang M, Zhang Y, Zhang L, Liu C, Khurshid S (2018) Deeproad: Gan-based metamorphic
1524 testing and input validation framework for autonomous driving systems. In: Proceedings
1525 of the 33rd ACM/IEEE International Conference on Automated Software Engineering,
1526 ACM, New York, NY, USA, ASE 2018, pp 132-142, DOI 10.1145/3238147.3238187, URL
1527 <http://doi.acm.org/10.1145/3238147.3238187>
- 1528 Zhang P, Wang J, Sun J, Dong G, Wang X, Wang X, Dong JS, Ting D (2020a) White-box
1529 fairness testing through adversarial sampling. In: Proceedings of the 42nd International
1530 Conference on Software Engineering, Association for Computing Machinery, New York,
1531 NY, USA, ICSE '20
- 1532 Zhang X, Xie X, Ma L, Du X, Hu Q, Liu Y, Zhao J, Sun M (2020b) Towards characterizing
1533 adversarial defects of deep learning software from the lens of uncertainty. In: Proceedings
1534 of the ACM/IEEE 42nd International Conference on Software Engineering, Association for
1535 Computing Machinery, New York, NY, USA, ICSE '20, p 739-751, DOI 10.1145/3377811.
1536 3380368, URL <https://doi.org/10.1145/3377811.3380368>
- 1537 Zhao J, Wang T, Yatskar M, Ordonez V, Chang KW (2017) Men also like shopping: Reduc-
1538 ing gender bias amplification using corpus-level constraints. In: Proceedings of the 2017
1539 Conference on Empirical Methods in Natural Language Processing, pp 2941-2951, URL
1540 <https://www.aclweb.org/anthology/D17-1319>
- 1541 Zhou B, Khosla A, Lapedriza A, Oliva A, Torralba A (2016) Learning deep features for discrim-
1542 inative localization. In: 2016 IEEE Conference on Computer Vision and Pattern Recogni-
1543 tion (CVPR), pp 2921-2929, DOI 10.1109/CVPR.2016.319
- 1544 Zhou ZQ, Sun L (2019) Metamorphic testing of driverless cars. Commun ACM 62(3):61-67,
1545 DOI 10.1145/3241979, URL <http://doi.acm.org/10.1145/3241979>
- 1546 Zoph B, Vasudevan V, Shlens J, Le QV (2018) Learning transferable architectures for scal-
1547 able image recognition. In: 2018 IEEE/CVF Conference on Computer Vision and Pattern
1548 Recognition, pp 8697-8710, DOI 10.1109/CVPR.2018.00907
- 1549